

Analysis of attosecond entanglement and coherence using feasible formulae

Yasuo Nabekawa^{✉*} and Katsumi Midorikawa[✉]

Attosecond Science Research Team, RIKEN Center for Advanced Photonics, 2-1 Hirosawa, Wako-shi, Saitama 351-0198, Japan



(Received 28 March 2023; accepted 10 July 2023; published 4 August 2023)

In recently published papers [M. J. J. Vrakking, *Phys. Rev. Lett.* **126**, 113203 (2021); *J. Phys. B* **55**, 134001 (2022)], Vrakking proposed an inventive scheme to control the entanglement or coherence of the vibrational states in a hydrogen molecular ion and a continuum electron, both of which were generated via the photoionization of a hydrogen molecule irradiated by a coherent pair of extreme ultraviolet (XUV) attosecond pulses and a few-femtosecond ultraviolet (UV) pulse. He clarified, for the first time to our knowledge, how the coherence of the XUV attosecond pulse pair is transferred to the molecular ion system accompanying a detached continuum electron by numerically solving a time-dependent Schrödinger equation (TDSE) governing the evolution of the ion and the electron in a rigorous manner. Nevertheless, it was not straightforwardly resolved how and why the specific characteristics of the resultant joint energy spectrogram emerged and how the entanglement or coherence was altered with the irradiation of the UV pulse. In this paper, we present an analytical solution of the TDSE using time-dependent perturbation theory, and we utilize the resultant solution to explain what causes the particular features in the entanglement or coherence between the electron and the ion spectra.

DOI: [10.1103/PhysRevResearch.5.033083](https://doi.org/10.1103/PhysRevResearch.5.033083)

I. INTRODUCTION

Photoelectron spectroscopy using light sources in the photon energy region of vacuum ultraviolet (VUV) or extreme ultraviolet (XUV) is a conventional tool for studying electronic and nuclear states in a molecule. This is mainly owing to the preservation of the energy conservation law among the photon energy of XUV light $\hbar\omega$, the ionization energy of an electron in a molecule I_p , and the kinetic energy (KE) of a detached electron K_e , so as to satisfy $K_e = \hbar\omega - I_p$, where \hbar and ω are Planck's constant divided by π and the angular frequency of the VUV/XUV light field, respectively. The details of the electronic and nuclear states in a molecule should be embedded in the structure of the photoelectron spectrum according to this simple relation when the VUV/XUV light field is monochromatic. This conventional measurement principle signifies that we can determine what happens in the molecule after the ionization without directly measuring the state of molecular ions left behind a continuum electron. For example, we implicitly assume that one H_2^+ molecular ion in the $v' = 2$ vibrational state should be generated from one neutral H_2 molecule upon the irradiation of XUV light with a photon energy of 21.21 eV whenever we detect one electron with a KE of 5.23 eV in an electron spectrometer [1]. The ability to determine the state of a physical system by observing the state of another physical system might originate from a kind of correlation or entanglement between the two systems, although we cannot determine whether the relation

between the two systems really corresponds to the technical term of “entanglement” defined in quantum physics [2] until we rigorously analyze the composite quantum system involving both the continuum state of an electron (e^-) and the quantum states in a molecular ion (M^+) generated after the irradiation of XUV light. This issue regarding quantum entanglement in a photoionization process may not have been noticed since photoelectron spectroscopy became one of the major tools in physics and chemistry more than half a century ago [3], because the energy conservation law of $K_e = \hbar\omega - I_p$ is a too obvious and sufficient reason to explain that the structure in the observed photoelectron spectrum originates from the quantum states of bound electrons in a molecule without explicitly considering the state of a continuum electron. In addition, the XUV light sources used in early photoelectron studies were monochromatic, which did not ensure the coherence of modern laser light sources; thus, it might not be straightforward to describe the interaction between such partially incoherent light and a molecular system.

The recent advent and progress of coherent ultrafast XUV light sources generated as a high-order harmonic (HH) field of intense femtosecond pulses in the visible-infrared photon energy region, which are called attosecond pulses, stimulated researchers' interest in another phenomenon in the photoionization process: The coherence among the quantum states in the ionized atoms or molecules. Some of the main concerns in this research field were to find how and when the coherence of the electronic states [5,6] emerged and disappeared owing to the electron correlations in an ion [7,8], the electron correlations involving a continuum electron [9], and the evolutions of nuclear states [10–12], the last of which might be regarded as “baths” that disturb the coherence in a general quantum system [13,14]. The major tool for analyzing the coherence in these studies was the reduced density matrix of the ionized molecule, in which the degree of the continuum state of a detached electron was partially traced from the density

*nabekawa@riken.jp

Published by the American Physical Society under the terms of the [Creative Commons Attribution 4.0 International license](https://creativecommons.org/licenses/by/4.0/). Further distribution of this work must maintain attribution to the author(s) and the published article's title, journal citation, and DOI.

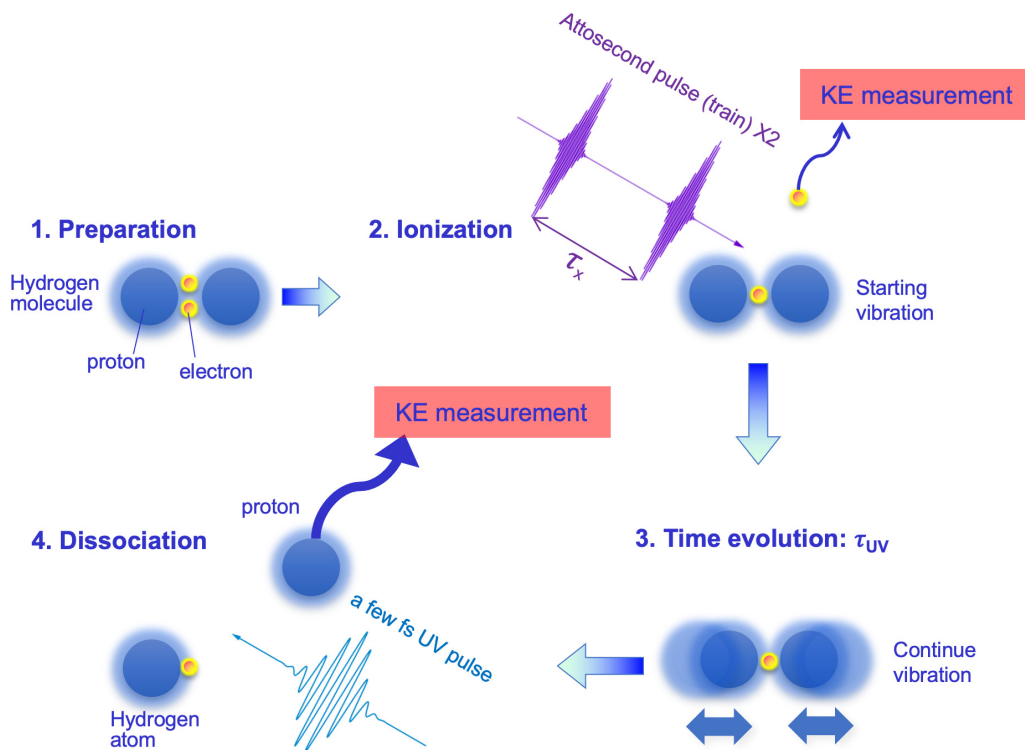


FIG. 1. Experimental scheme to confirm the coherence between the continuum state of a detached electron and the vibrational state of H_2^+ shown in Ref. [4].

matrix. Thus, it was natural for researchers to be interested in the entanglement between the ionized molecule and the detached electron [8,15–17] because the reduced density matrix was also the principal measure that determines the degree of entanglement [2]. Nevertheless, there was no notable study on photoelectron spectroscopy under the consideration of the coherence or entanglement between the ionized molecule and the continuum electron. This might be because it was apparent that the energies of the vibrational states could not be resolved in a photoelectron spectrum with the irradiation of broadband XUV attosecond pulses.

In 2021, Vrakking shed new light on this research field [4]. The key idea of his study was to irradiate a molecule with a pair of XUV attosecond pulses followed by an ultraviolet (UV) pulse, and detect an ejected electron and a fragment molecular ion in coincidence. In his study, coherence in a broad frequency range and a pulse duration sufficiently shorter than the period of the nuclear motion, which are specific characteristics of an XUV attosecond pulse as opposed to those of a monochromatic XUV light source used for precision photoelectron spectroscopy, played a crucial role in determining the coherence or entanglement between the state of a continuum electron and that of the molecular ion in the composite quantum system, $e^- \otimes M^+$.

A schematic figure of the experiment Vrakking proposed is shown in Fig. 1. In this scheme, a hydrogen molecule, H_2 , is provided as a target, then a pair of XUV attosecond pulses with a time separation of τ_x is irradiated to photoionize the H_2 target. The hydrogen molecular ion, H_2^+ , generated immediately after the photoionization, starts vibrating, while the detached electron should be sent to an electron spectrometer to resolve the KE. After a delay time of $\tau_u > \tau_x$

from the time of the first XUV attosecond pulse irradiation, a few-fs UV pulse is irradiated to dissociate the vibrating H_2^+ into a hydrogen atom, H, and a proton, H^+ . The KE of the proton is measured using an ion spectrometer in coincidence with the detection event of a photoelectron such that the detected photoelectron and proton originate from the same hydrogen molecule. This coincident measurement of the KE of the photoelectron with that of the proton can provide the joint energy spectrum (JES) of the electron and proton, which should indicate how entanglement and coherence are altered in the composite quantum system. In fact, Vrakking provided clear evidence of the coherence between the photoelectron and the ion at $\tau_x = 12.1$ fs by demonstrating that the phase of the spectral interference fringes of the photoelectron was altered upon changing the delay of the UV pulse τ_u , although the UV pulse was always irradiated after the detachment of the electron. The interchange of coherence and entanglement was also found as a variation of the purity of the reduced density matrix in accordance with the change in τ_x , and many such fruitful outcomes were obtained from this study.

Nevertheless, we do not clearly understand why and how the spectral features of the JES could be controlled via τ_x because previous studies [4,18] were based on numerical calculation to solve the time-dependent Schrödinger equation (TDSE), and the relations among the spectral interference of the continuum electron, the vibrational period of H_2^+ , and the kinetic energy release (KER) of the dissociating $H + H^+$ were not explicitly resolved. Thus, it will be useful to find an analytical model for describing the JES and revealing the origin of its modulation structure. In addition, the entanglement or coherence between the continuum electron and the

dissociating $H + H^+$ generated after UV pulse irradiation is still unknown.

In this paper, we report on the derivation of an analytical formula providing the approximate solution of the TDSE by applying perturbation theory. The JES calculated using this formula properly reproduces those obtained by numerical calculation in Ref. [4]. We also demonstrate that the JES without resolving the KER of the proton should be sufficient to exhibit the coherence of the composite system, $e^- \otimes H_2^+$, through the numerical integration of the KER of the proton, taking advantage of the low calculation cost of the analytical formula. We clarify how the modulation structure of the KE spectrum of the electron changes upon changing τ_u by employing the simplified formula.

In the following two sections, we apply the first- and second-order solutions of the TDSE obtained from the time-dependent perturbation theory (described in Appendix A) to approximate the one-photon (Sec. II) and two-photon (Sec. III) transition amplitudes so as to reproduce the $e^- \otimes H_2^+$ system under the experimental scheme depicted in Fig. 1. Then, the JES and the KE spectra of the electron calculated from the obtained formula are exhibited. After describing the analysis of the modulation structure of the KE spectra, we discuss the degree of coherence or entanglement by evaluating the purity and von Neumann entropy of the reduced density matrix after the irradiation of the XUV pulse pair (Sec. II) and also by evaluating those after the irradiation of the UV pulse (Sec. III). A summary is given in the final section (Sec. IV).

II. ONE-PHOTON INTERACTION

A. General form of the state vector

In Appendix A, we provide detailed descriptions concerning how we have derived the general formulas of the electronic state vectors of the molecular system interacting with optical fields in accordance with the conventional time-dependent perturbation theory and the Born-Oppenheimer (BO) approximation, under which the electronic state vector $|\Psi(\mathbf{R}; t)\rangle$ given by Eq. (A20) in Appendix A parametrically depends on the nuclear coordinates \mathbf{R} . The notations used in the following equations are all defined in Appendix A.

In this section, we focus on the second term on the right-hand side of Eq. (A20), which describes the state vector evolved with a linear contribution of the optical electric field; thus, we identify this term as the state vector with the one-photon interaction as follows:

$$|\Psi^{(1)}(\mathbf{R}; t)\rangle = \frac{1}{i\hbar} \int_{t_0}^t dt_1 \int d^3M \mathbf{R}_1 \int d^3M \mathbf{R}_2 e^{\frac{i\hbar(\mathbf{R}_2)}{\hbar}(t-t_1)} \hat{I}(\mathbf{R}; \mathbf{R}_1) \times \hat{V}(t_1) \hat{I}(\mathbf{R}_1; \mathbf{R}_2) e^{\frac{i\hbar(\mathbf{R}_2)}{\hbar}(t_1-t_0)} |\Psi(\mathbf{R}_2; t_0)\rangle, \quad (1)$$

where we introduce the identity operator $\hat{I}(\mathbf{R}; \mathbf{R}')$ satisfying $\int d^3M \mathbf{R}' \hat{I}(\mathbf{R}; \mathbf{R}') |\Psi(\mathbf{R}'; t)\rangle = |\Psi(\mathbf{R}; t)\rangle$ for any $|\Psi(\mathbf{R}; t)\rangle$. If the eigenstate vectors of molecular Hamiltonian $\hat{H}(\mathbf{R})$, which may be written as $|\Psi_k(\mathbf{R})\rangle$, form the complete set, the identity matrix takes the form of $\hat{I}(\mathbf{R}; \mathbf{R}') = \sum_k |\Psi_k(\mathbf{R})\rangle \langle \Psi_k(\mathbf{R}')|$, where k is the quantum number identifying the electronic and nuclear states, and all the states of all charged molecular ions and detached continuum electrons should be included in the

summation or integration if we define $\hat{I}(\mathbf{R}; \mathbf{R}')$ in a rigorous manner. However, here we consider only the state vectors of a neutral molecule and a singly charged molecular ion accompanying a continuum electron, and thus we approximate $\hat{I}(\mathbf{R}; \mathbf{R}')$ as

$$\hat{I}(\mathbf{R}; \mathbf{R}') \simeq \hat{P}(\mathbf{R}; \mathbf{R}') + \hat{P}^+(\mathbf{R}; \mathbf{R}'), \quad (2)$$

which is the summation of the projection operator to the state of a neutral molecule, $\hat{P}(\mathbf{R}; \mathbf{R}')$, and that to the state of a molecular ion accompanying a continuum electron, $\hat{P}^+(\mathbf{R}; \mathbf{R}')$. These operators are defined in Eqs. (A8) and (A17) in Appendix A, respectively.

We assume the initial state to be the ground electronic and nuclear states of a neutral molecule, $|\Psi(\mathbf{R}_2; t_0)\rangle = |\Psi_g^0(\mathbf{R}_2)\rangle$, allowing us to neglect the contribution of $\hat{P}^+(\mathbf{R}_1; \mathbf{R}_2)$ in $\hat{I}(\mathbf{R}_1; \mathbf{R}_2)$ on the right-hand side of $\hat{V}(t_1)$ in Eq. (1) when we substitute Eq. (2) into Eq. (1). As a result, $|\Psi^{(1)}(\mathbf{R}; t)\rangle$ is divided into two vectors, one of which represents the excited state of a neutral molecule $|\Psi_n^{(1)}(\mathbf{R}; t)\rangle$ and the other of which is the state vector of the molecular ion accompanying a continuum electron $|\Phi_i^{+(1)}(\mathbf{R}; t)\rangle$, as shown in the following equations:

$$|\Psi_n^{(1)}(\mathbf{R}; t)\rangle = \frac{1}{i\hbar} \sum_{\alpha} \sum_{jv} |\Psi_{\alpha}^v(\mathbf{R})\rangle e^{-i\omega_{\alpha}^v t} \mu_{\alpha g}^v \tilde{E}(\omega_{\alpha}^v - \omega_g^0), \quad (3)$$

$$|\Phi_i^{+(1)}(\mathbf{R}; t)\rangle = \frac{1}{i\hbar} \sum_{\beta} \sum_{jv'} \int_0^{\infty} d\omega_e |\Psi_{\beta}^{+v'}(\mathbf{R})\rangle |\psi_{c_{\beta}}(\omega_e)\rangle \times e^{-i(\omega_{\beta}^{+v'} + \omega_e)t} \mu_{\beta g}^{+v'}(\omega_e) \tilde{E}(\omega_{\beta}^{+v'} + \omega_e - \omega_g^0). \quad (4)$$

Here, we define the transition dipole moment to the α -electronic and v th vibrational state in the neutral molecule as $\mu_{\alpha g}^v \equiv \int d^3M \mathbf{R}_1 \langle \Psi_{\alpha}^v(\mathbf{R}_1) | \hat{\mu} | \Psi_g^0(\mathbf{R}_1) \rangle = \int d^3M \mathbf{R}_1 \phi_{\alpha}^{v*}(\mathbf{R}_1) \phi_g^0(\mathbf{R}_1) \langle \psi_{e_{\alpha}}(\mathbf{R}_1) | \hat{\mu} | \psi_{e_g}(\mathbf{R}_1) \rangle$ and that to the β -electronic and v' th vibrational state in the molecular ion accompanying a continuum electron with a KE of $\hbar\omega_e$ as $\mu_{\beta g}^{+v'}(\omega_e) \equiv \int d^3M \mathbf{R}_1 \langle \Psi_{\beta}^{+v'}(\mathbf{R}_1) | \langle \psi_{c_{\beta}}(\omega_e) | \hat{\mu} | \Psi_g^0(\mathbf{R}_1) \rangle = \int d^3M \mathbf{R}_1 \phi_{\beta}^{+v'*}(\mathbf{R}_1) \phi_g^0(\mathbf{R}_1) \langle \psi_{e_{\beta}}^+(\mathbf{R}_1) | \langle \psi_{c_{\beta}}(\omega_e) | \hat{\mu} | \psi_{e_g}(\mathbf{R}_1) \rangle$. Both dipole moments are obtained by integrating the overlap of the nuclear wave functions multiplied by the electronic transition dipole moment with respect to the nuclear coordinates as usual. The angular frequencies of ω_{α}^v and $\omega_{\beta}^{+v'}$ are obtained by dividing the eigenenergies of E_{α}^v in Eq. (A6) and $E_{\beta}^{+v'}$ in Eq. (A14) by \hbar , respectively. We have omitted the constant phase factor $e^{i\omega_g^0 t_0}$ from Eqs. (3) and (4) and approximated the time integration in terms of t_1 as the Fourier amplitude of the positive frequency part of the complex optical electric field given by Eq. (A19), $\int_{t_0}^t dt_1 E(t_1) e^{i\Omega t_1} \simeq \int_{-\infty}^{\infty} dt_1 E(t_1) e^{i\Omega t_1} \equiv \tilde{E}(\Omega)$, because we can expect that the magnitude square peaks of the electric fields of the first and second XUV pulses and that of the UV pulse ($|E_x(t_1)|^2$, $|E_x(t_1 - \tau_x)|^2$, and $|E_u(t_1 - \tau_u)|^2$) will arrive at the interaction region long after the initial time t_0 and far before the present time t . The inverse Fourier transform (FT) should be performed using $E(t) = \frac{1}{2\pi} \int d\Omega \tilde{E}(\Omega) e^{-i\Omega t}$ from the definition of the FT mentioned above. The actual form

of $\tilde{E}(\Omega)$ can be given by $\tilde{E}(\Omega) = \tilde{E}_x(\Omega; \tau_x) + \tilde{E}_u(\Omega; \tau_u) = \tilde{E}_x(\Omega)(1 + e^{i\Omega\tau_x}) + \tilde{E}_u(\Omega)e^{i\Omega\tau_u}$ from Eq. (A19), where $\tilde{E}_x(\Omega)$ and $\tilde{E}_u(\Omega)$ are the Fourier amplitudes of $E_x(t)$ and $E_u(t)$, respectively. Note that these Fourier amplitudes may be expressed as

$$\tilde{E}_x(\Omega) = \tilde{A}_x(\Omega - \omega_x), \quad (5)$$

$$\tilde{E}_u(\Omega) = \tilde{A}_u(\Omega - \omega_u) \quad (6)$$

when we adopt a single-peak envelope as an XUV pulse with a carrier angular frequency of ω_x and a UV pulse with a carrier angular frequency of ω_u . If we assume that the XUV optical field originates from the HH pulse called the attosecond pulse train (APT), $\tilde{E}_x(\Omega)$ can be expressed as $\tilde{E}_x(\Omega) = \sum_n \tilde{A}_{x_{2n+1}}(\Omega - \omega_{2n+1})$, where the odd number $2n + 1$ denotes the harmonic order and the carrier angular frequency of the $(2n + 1)$ th harmonic pulse is denoted as ω_{2n+1} . The magnitudes of the Fourier amplitudes of the temporal envelopes, $\tilde{A}_x(\Omega)$, $\tilde{A}_{x_{2n+1}}(\Omega)$, and $\tilde{A}_u(\Omega)$, should all exhibit a peak around $\Omega = 0$.

We restrict ourselves to considering the ionization process bringing about the state vector $|\Psi_i^{(1)}(\mathbf{R}; t)\rangle$ in Eq. (4) to analyze the entanglement or coherence between the molecular ion and the continuum electron described by using a composite basis set of $|\Psi_{\beta}^{+v'}(\mathbf{R})\rangle|\psi_{c\beta}(\omega_e)\rangle$. The excited states in the neutral molecule constituting $|\Psi_n^{(1)}(\mathbf{R}; t)\rangle$ in Eq. (3) play a role in the nonlinear excitation/ionization process, determined as high-order terms in the perturbative solution. We also only consider a single-peak XUV pulse described in Eq. (5) for simplicity.

B. Entanglement or coherence of the $e^- \otimes \text{H}_2^+$ system

We simplify the state vector $|\Psi_i^{(1)}(\mathbf{R}; t)\rangle$ to express the $e^- \otimes \text{H}_2^+$ system. The nuclear coordinate \mathbf{R} can be reduced to a relative position vector from one proton to another, and the rotational state is assumed to be the ground state. The most relevant electronic state in the $e^- \otimes \text{H}_2^+$ system is the $1s\sigma_g$ ground state of H_2^+ ; thus, we omit the summation with suffix β and replace β with g' in Eq. (4). We also neglect the dissociative nuclear wave function in the $1s\sigma_g$ ground state and only take the discrete vibrational numbers into account. The state vector is renormalized such that the trace of the density matrix, which will later be needed to evaluate the degree of entanglement, should coincide with unity. We can neglect the contribution of the UV optical field because we assume that the photon energy of the UV optical field is lower than the ionization energy, namely, $\omega^{+v'} - \omega_g^0 > \omega_u$. This allows us to evaluate the magnitude of the Fourier amplitude of the UV optical field $\tilde{E}_u(\omega^{+v'} + \omega_e - \omega_g^0) = \tilde{A}_u(\omega_e + \omega^{+v'} - \omega_g^0 - \omega_u) \simeq 0$ in the range of $\omega_e \geq 0$.

Then, the state vector of the $e^- \otimes \text{H}_2^+$ system is given by

$$|\Psi_i^{(1)}(\mathbf{R}; t)\rangle = C \sum_{v'} \int_0^\infty d\omega_e |\Psi_{1s\sigma_g}^{+v'}(\mathbf{R})\rangle |\psi_c(\omega_e)\rangle e^{-i(\omega^{+v'} + \omega_e)t} \times \mu_{1s\sigma_g}^{+v'}(\omega_e) \tilde{A}_x(\omega^{+v'} + \omega_e - \omega_g^0 - \omega_x; \tau_x), \quad (7)$$

where C is a normalization constant and we define $\tilde{A}_x(\Omega - \omega_x; \tau_x)$ as $\tilde{A}_x(\Omega - \omega_x; \tau_x) \equiv \tilde{A}_x(\Omega - \omega_x)(1 + e^{i\Omega\tau_x}) = \tilde{E}_x(\Omega)(1 + e^{i\Omega\tau_x}) = \tilde{E}_x(\Omega; \tau_x)$.

According to a standard textbook of quantum computation and information [2], and as already demonstrated with respect to the $e^- \otimes \text{H}_2^+$ system in Ref. [18], the reduced density matrix of the composite system composed of pure states plays a significant role in evaluating the degree of entanglement. In our model, we disregard the mixture of the vibrationally and rotationally excited states in the initial neutral molecule. Thus, the density matrix with the one-photon interaction can be simply expressed as the following pure state density matrix:

$$\hat{\rho}_i^{(1)}(\mathbf{R}', \mathbf{R}''; t) = |\Psi_i^{(1)}(\mathbf{R}'; t)\rangle \langle \Psi_i^{(1)}(\mathbf{R}''; t)|, \quad (8)$$

where $|\Psi_i^{(1)}(\mathbf{R}; t)\rangle$ is given by Eq. (7). The reduced density matrix with respect to the nuclear degree of freedom $\hat{\rho}_{\text{nclr}}^{(1)}(\mathbf{R}', \mathbf{R}''; t)$ is obtained by calculating $\int_0^\infty d\omega_e \langle \psi_c(\omega_e) | \hat{\rho}_i^{(1)}(\mathbf{R}', \mathbf{R}''; t) | \psi_c(\omega_e) \rangle$.

The $v'v''$ element of $\hat{\rho}_{\text{nclr}}^{(1)}(\mathbf{R}', \mathbf{R}''; t)$ is given by $\int d^3\mathbf{R}' \int d^3\mathbf{R}'' \langle \Psi_{1s\sigma_g}^{+v'}(\mathbf{R}'; t) | \hat{\rho}_{\text{nclr}}^{(1)}(\mathbf{R}', \mathbf{R}''; t) | \Psi_{1s\sigma_g}^{+v''}(\mathbf{R}''; t) \rangle$,

where $|\Psi_{1s\sigma_g}^{+v'}(\mathbf{R}; t)\rangle \equiv |\Psi_{1s\sigma_g}^{+v'}(\mathbf{R})\rangle e^{-i\omega^{+v'}t}$ is the asymptotic form of the wave function of the molecular ion at time t . As a result, we obtain the $v'v''$ element of the reduced density matrix $\rho_{\text{ion},v'v''}^{(1)}$ as follows:

$$\rho_{\text{ion},v'v''}^{(1)} = |C|^2 \int_0^\infty d\omega_e \mu_{1s\sigma_g}^{+v'}(\omega_e) \mu_{1s\sigma_g}^{+v''*}(\omega_e) \tilde{A}_x(\omega^{+v'} + \omega_e - \omega_g^0 - \omega_x; \tau_x) \tilde{A}_x^*(\omega^{+v''} + \omega_e - \omega_g^0 - \omega_x; \tau_x). \quad (9)$$

The normalization constant is obtained as follows by imposing $\sum_{v'} \rho_{\text{ion},v'v'}^{(1)} = 1$:

$$|C|^2 = \left[\sum_{v'} \int_0^\infty d\omega_e |\mu_{1s\sigma_g}^{+v'}(\omega_e)|^2 \times |\tilde{A}_x(\omega^{+v'} + \omega_e - \omega_g^0 - \omega_x; \tau_x)|^2 \right]^{-1}. \quad (10)$$

The reduced density matrix described in Eq. (9) is the same as that in Eq. (33) in Ref. [18] introduced by Vrakking without the description for the detailed derivation process, and thus we have shown that this equation is correct under the condition that the perturbative solution is valid.

The reduced density matrix with respect to the continuum electron is calculated by the formula $\hat{\rho}_e^{(1)}(t) = \sum_{v'} \int d^3\mathbf{R}' \int d^3\mathbf{R}'' \langle \Psi_{1s\sigma_g}^{+v'}(\mathbf{R}'; t) | \hat{\rho}_i^{(1)}(\mathbf{R}', \mathbf{R}''; t) | \Psi_{1s\sigma_g}^{+v''}(\mathbf{R}''; t) \rangle$, and we obtain its $\omega'_e - \omega_e$ element $\rho_e^{(1)}(\omega'_e, \omega_e) = \langle \psi_c(\omega'_e; t) | \hat{\rho}_e^{(1)}(t) | \psi_c(\omega_e; t) \rangle$ as

$$\rho_e^{(1)}(\omega'_e, \omega_e) = |C|^2 \sum_{v'} \mu_{1s\sigma_g}^{+v'}(\omega'_e) \mu_{1s\sigma_g}^{+v''*}(\omega_e) \tilde{A}_x(\omega^{+v'} + \omega'_e - \omega_g^0 - \omega_x; \tau_x) \tilde{A}_x^*(\omega^{+v''} + \omega_e - \omega_g^0 - \omega_x; \tau_x), \quad (11)$$

which is independent of t because we define $|\psi_c(\omega_e; t)\rangle \equiv |\psi_c(\omega_e)\rangle e^{-i\omega_e t}$. We show a trivial example of the reduced

density matrix $\hat{\rho}_e^{(1)}(t)$ leading to a physical quantity. The projection operator $\hat{P}(\omega_e) = |\psi_c(\omega_e)\rangle\langle\psi_c(\omega_e)|$ yields the probability of finding a continuum electron with a KE of $\hbar\omega_e$ by $\text{Tr}\{\hat{\rho}_e^{(1)}(t)\hat{P}(\omega_e)\} = \rho_e^{(1)}(\omega_e, \omega_e) = |C|^2 \sum_{v'} |\mu_{1s\sigma_g}^{+v'}(\omega_e)|^2 |\tilde{A}_x(\omega^{+v'} + \omega_e - \omega_g^0 - \omega_x; \tau_x)|^2$, which is indeed proportional to the photoelectron spectrum.

Before using the reduced density matrix $\rho_{\text{ion},v',v''}^{(1)}$ in Eq. (9) to evaluate the entanglement, we give an explicit form of the state vector apparently expressing the entanglement between the molecular ion and the continuum electron under the extreme condition that a single XUV electric field with an angular frequency of ω_x and an infinitely narrow bandwidth described as $\tilde{A}_x(\omega^{+v'} + \omega_e - \omega_g^0 - \omega_x; \tau_x = 0) = 2\delta\omega\tilde{A}_{x0}\delta(\omega_e + \omega^{+v'} - \omega_g^0 - \omega_x)$ is irradiated. Substituting this electric field into Eq. (7), we obtain the state vector

$$|\Psi_i^{(1)}(\mathbf{R}; t)\rangle \propto \sum_{v'} \mu_{1s\sigma_g}^{+v'}(\omega_e^{v'}) |\Psi_{1s\sigma_g}^{+v'}(\mathbf{R})\rangle |\psi_c(\omega_e^{v'})\rangle, \quad (12)$$

where $\omega_e^{v'} \equiv \omega_x - (\omega^{+v'} - \omega_g^0)$. Equation (12) is similar to a typical form of the Schmidt decomposition [2] of the composite state if the dipole moment $\mu_{1s\sigma_g}^{+v'}(\omega_e^{v'})$ is a non-negative real number, and we impose the normalization condition. Thus, we determine that the state of the molecular ion is quasientangled with the state of the continuum electron from this equation. Researchers have been making use of this fact for the conventional photoelectron spectroscopy of molecules since the first observation of the structure involving discrete peaks in the photoelectron spectrum of H_2 more than half a century ago [1]. When an electron with a KE of $\hbar\omega_e^{v'}$ is detected, we tacitly assume that the state of the H_2^+ ion left behind is the v' th vibrational state. The possible determination of the state of one system involved in a composite system by the measurement of the state of another system is the same as the property of the Bell states, which are well-known examples showing entanglement [2].

Next, we investigate the purity of the square of the reduced density matrix Pu , or the von Neumann entropy \mathbf{S} , as an indicator of entanglement. We assume that the dipole moment does not significantly change in the range of the frequency bandwidth of $\tilde{A}_x(\Omega - \omega_x)$, and the electronic states can be

approximated to those at the equilibrium nuclear position of the ground vibrational state in the $X^1\Sigma_g^+$ state of H_2 , \mathbf{R}_{eq} , allowing us to apply the following approximation:

$$\mu_{1s\sigma_g}^{+v'}(\omega_e) \simeq \int d^3\mathbf{R} \phi_{1s\sigma_g}^{+v'*}(\mathbf{R}) \phi_X^0(\mathbf{R}) \langle \psi_{e_{1s\sigma_g}}^+(\mathbf{R}_{\text{eq}}) | \times \langle \psi_c(\omega_e^{v'}) | \hat{\mu} | \psi_{e_x}(\mathbf{R}_{\text{eq}}) \rangle \equiv \mu^{+v'}, \quad (13)$$

where $\phi_X^0(\mathbf{R})$ is the ground vibrational wave function in the $X^1\Sigma_g^+$ state of H_2 and $\phi_{1s\sigma_g}^{+v'*}(\mathbf{R})$ is the v' th vibrational wave function in the $1s\sigma_g$ state of H_2^+ . The dipole moment becomes the product of the overlap integral between the vibrational wave functions and the electronic dipole at \mathbf{R}_{eq} to generate a continuum electron with a KE of $\hbar\omega_e^{v'}$, and thus it can be excluded from the ω_e integral in Eq. (9). By applying the approximation of Eq. (13) to Eq. (9), we obtain the following reduced density matrix of the nuclei:

$$\rho_{\text{ion},v',v''}^{(1)}(\tau_x) = |C|^2 \mu^{+v'} \mu^{*+v''} \int d\omega_e \tilde{A}_x(\omega_e - \omega_e^{v'}) \tilde{A}_x^*(\omega_e - \omega_e^{v''}) \times \{1 + e^{i(\omega_e + \Delta\omega^{v'})\tau_x}\} \{1 + e^{-i(\omega_e + \Delta\omega^{v''})\tau_x}\}. \quad (14)$$

Here, we define the ionization energy from the ground electronic-vibrational state in the neutral molecule to the v' th vibrational state in the $1s\sigma_g$ state as $\hbar\Delta\omega^{v'} \equiv \hbar(\omega^{+v'} - \omega_g^0)$, and we extend the lower limit of the ω_e integral to $-\infty$ by assuming that the photon energy of the XUV field is sufficiently high to satisfy the condition $\omega_e^{v'} = \omega_x - \Delta\omega^{v'} \gg \delta\Omega$, where $\delta\Omega$ is the bandwidth of $\tilde{A}_x(\Omega)$. We explicitly show the dependence of the delay between the XUV pulse pair τ_x in the reduced density matrix.

In accordance with Ref. [18], we also employ the model of the Gaussian envelope function as $\tilde{A}_x(\Omega)$:

$$\tilde{A}_x(\Omega) = \tilde{A}_0 e^{-\frac{\Omega^2}{\delta\Omega^2} + i\frac{\ddot{\phi}}{2}\Omega^2}, \quad (15)$$

where $\ddot{\phi}$ is the group delay dispersion (GDD) of the XUV pulse. Substituting Eq. (15) into Eq. (14), we specify the following form of the reduced density matrix:

$$\rho_{\text{ion},v',v''}^{(1)}(\tau_x) = |C'|^2 \mu^{+v'} \mu^{*+v''} e^{-\frac{1}{2\delta\Omega^2}(\omega^{v'} - \omega^{v''})^2} [e^{-\frac{\delta\Omega^2}{8}\{\ddot{\phi}(\omega^{v'} - \omega^{v''})\}^2} \{1 + e^{i(\omega^{v'} - \omega^{v''})\tau_x}\} + e^{-\frac{\delta\Omega^2}{8}\{\ddot{\phi}(\omega^{v'} - \omega^{v''}) + \tau_x\}^2} e^{i\{\omega_x + \frac{1}{2}(\omega^{v'} - \omega^{v''})\}\tau_x} + e^{-\frac{\delta\Omega^2}{8}\{\ddot{\phi}(\omega^{v'} - \omega^{v''}) - \tau_x\}^2} e^{-i\{\omega_x - \frac{1}{2}(\omega^{v'} - \omega^{v''})\}\tau_x}]. \quad (16)$$

Here, $|C'|^2$ is related to $|C|^2$ as $|C'|^2 = |C|^2 \sqrt{\frac{\pi}{2}} |\tilde{A}_0|^2 \Delta\Omega$ and should be equal to the following form:

$$|C'|^2 = [2N \langle |\mu^+|^2 \rangle \{1 + e^{-\frac{\delta\Omega^2}{8}\tau_x^2} \cos(\omega_x \tau_x)\}]^{-1}, \quad (17)$$

by imposing the normalization condition of $\sum_{v'=0}^{N_v-1} \rho_{\text{ion},v',v'}^{(1)} = 1$. We define the number of vibrational states as N_v and express the absolute square average of the transition dipole as $\langle |\mu^+|^2 \rangle = \frac{1}{N_v} \sum_{v'=0}^{N_v-1} |\mu^{+v'}|^2$. We also utilize the relation $\Delta\omega^{v'} - \Delta\omega^{v''} = \omega^{v'} - \omega^{v''}$. When the delay τ_x is equal to zero

or, equivalently, a single XUV pulse is irradiated, $\rho_{\text{ion},v',v''}^{(1)}(\tau_x = 0)$ is reduced to the following simple formula:

$$\rho_{\text{ion},v',v''}^{(1)}(0) = \frac{\mu^{+v'} \mu^{*+v''}}{N_v \langle |\mu^+|^2 \rangle} e^{-\frac{1}{2\delta\Omega^2}(\omega^{v'} - \omega^{v''})^2} e^{-\frac{\delta\Omega^2}{8}\{\ddot{\phi}(\omega^{v'} - \omega^{v''})\}^2}. \quad (18)$$

We find from Eq. (16) [from Eq. (18)] that the off-diagonal elements of $\rho_{\text{ion},v',v''}^{(1)}(\tau_x)$ can survive for $\tau_x > 0$ (for $\tau_x = 0$) only if the bandwidth $\delta\Omega$ is sufficiently large to satisfy the

condition $\delta\Omega \gg |\omega^{v'} - \omega^{v''}|$ and the GDD $\ddot{\phi}$ is sufficiently small to satisfy the condition $|\ddot{\phi}(\omega^{v'} - \omega^{v''})| \ll \delta\Omega^{-1}$. The off-diagonal elements disappear under the opposite extreme condition of a narrow bandwidth or large GDD, resulting in the mixed state losing coherence. This conclusion simply implies that the vibrational state in the $1s\sigma_g$ state is coherent only when the pulse duration of the XUV pulse is sufficiently shorter than the principal vibrational period.

In fact, we identify the asymptotic forms of $\rho_{\text{ion}_{v'v''}}^{(1)}(0)$ under the two extreme conditions mentioned above. Setting $\ddot{\phi} = 0$ and $\delta\Omega \rightarrow \infty$, the Gaussian function $e^{-\frac{1}{2\delta\Omega^2}(\omega^{v'} - \omega^{v''})^2}$ approaches unity independently of v', v'' , and thus $\rho_{\text{ion}_{v'v''}}^{(1)}(0) \rightarrow \mu^{+v'}\mu^{*+v''}/(N_v\langle|\mu^+|^2\rangle)$ or $\hat{\rho}_{\text{ion}}^{(1)}(0) \rightarrow \bar{\mu} : \bar{\mu}^\dagger$, where we define the normalized vector $\bar{\mu} \equiv (\mu^0, \mu^1, \dots, \mu_{N_v-1})^T / \sqrt{N_v\langle|\mu^+|^2\rangle}$ satisfying $\bar{\mu}^\dagger \cdot \bar{\mu} = 1$ to describe the matrix $\hat{\rho}_{\text{ion}}^{(1)}(0)$. Apparently, the state of H_2^+ is pure and the $e^- \otimes \text{H}_2^+$ system is coherent under this extreme condition because $\hat{\rho}_{\text{ion}}^{(1)}(0)$ is expressed as a sum of only one outer product of the vector $\bar{\mu}$; thus, the von Neumann entropy is $\mathbf{S} = -1 \cdot \log_2(1) = 0$ and the purity is $\text{Pu} = \bar{\mu}^\dagger \hat{\rho}_{\text{ion}}^{(1)}(0) \bar{\mu} = 1$.

On the other hand, the product of the Gaussian functions on the right-hand side of Eq. (18) leads to $\delta_{v'v''}$ when $\delta\Omega$ is reduced to zero or $|\delta\Omega\ddot{\phi}|$ approaches infinity; thus, we obtain the following asymptotic form of $\rho_{\text{ion}_{v'v''}}^{(1)}(0)$:

$$\begin{aligned} \rho_{\text{ion}_{v'v''}}^{(1)}(0) &\rightarrow \delta_{v'v''} |\mu^{+v'}|^2 / (N_v \langle |\mu^+|^2 \rangle) \\ &= \delta_{v'v''} p_{v'} (\delta\Omega \rightarrow 0 \text{ or } |\delta\Omega\ddot{\phi}| \rightarrow \infty), \end{aligned} \quad (19)$$

where $p_{v'} = |\mu^{+v'}|^2 / (N_v \langle |\mu^+|^2 \rangle)$ is the transition probability from the ground vibrational state in the $X^1\Sigma_g^+$ state of the neutral H_2 to the v' th vibrational state of the $1s\sigma_g$ state of H_2^+ . The reduced density matrix $\rho_{\text{ion}_{v'v''}}^{(1)}(0)$ is a diagonal matrix, and thus the square of the reduced density matrix is also diagonal, whose $v'v''$ element is given by $\hat{\rho}_{\text{ion}_{v'v''}}^{(1)2}(0) = \delta_{v'v''} p_{v'}^2$. Therefore, we evaluate $\mathbf{S} = -\sum_{v'=0}^{N_v-1} p_{v'}^2 \log_2(p_{v'}^2) > 0$ and $\text{Pu} = \sum_{v'=0}^{N_v-1} p_{v'}^2 < 1$, resulting in the mixed state of H_2^+ and the entanglement of the $e^- \otimes \text{H}_2^+$ system. When we approximate $\mu^{+v'}$ as proportional to the overlap integral between the ground vibrational state wave function in the $X^1\Sigma_g^+$ state of the neutral H_2 and the v' th vibrational state wave function in the $1s\sigma_g$ state of H_2^+ , we obtain $\mathbf{S} \simeq 3$ and $\text{Pu} \simeq 0.2$, respectively, under this extreme condition. Using Eq. (16), we can qualitatively evaluate the evolution of the entanglement upon changing the delay between the two XUV pulses τ_x . When the delay τ_x is sufficiently larger than the pulse duration so as to satisfy $|\delta\Omega\tau_x| \gg 1$, the second and third terms in the square brackets of Eq. (16) can be neglected and the reduced density matrix $\rho_{\text{ion}_{v'v''}}^{(1)}(\tau_x)$ is simplified to

$$\begin{aligned} \rho_{\text{ion}_{v'v''}}^{(1)}(\tau_x) &\rightarrow \frac{\mu^{+v'}\mu^{*+v''}}{2N_v\langle|\mu^+|^2\rangle} e^{-\frac{1}{2\delta\Omega^2}(\omega^{v'} - \omega^{v''})^2} \{1 + e^{i(\omega^{v'} - \omega^{v''})\tau_x}\}, \\ &(\ddot{\phi} = 0 \text{ and } |\delta\Omega\tau_x| \gg 1). \end{aligned} \quad (20)$$

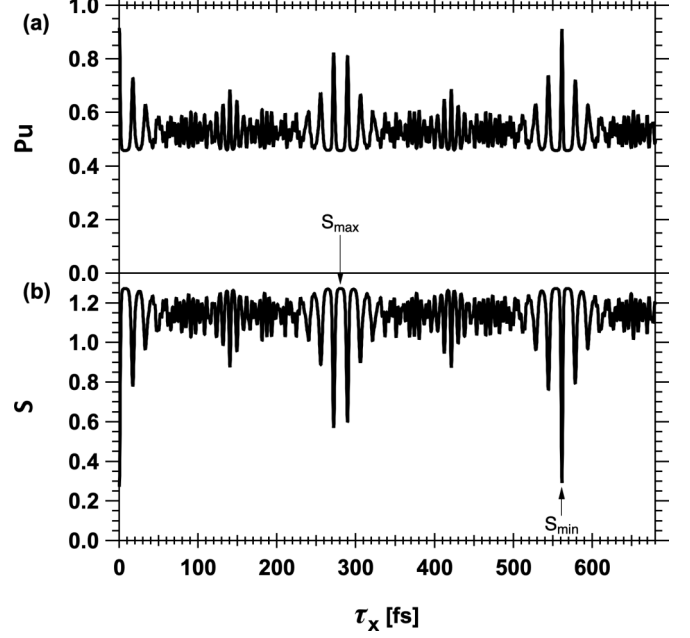


FIG. 2. (a) Evolution of the purity of the reduced density matrix $\rho_{\text{ion}_{v'v''}}^{(1)}(\tau_x)$ upon changing the delay between the XUV pulse pair. (b) Evolution of the von Neumann entropy of $\rho_{\text{ion}_{v'v''}}^{(1)}(\tau_x)$. One of the local maxima and one of the local minima are indicated with arrows.

We set the GDD to zero to assume a Fourier limit XUV pulse pair to obtain Eq. (20). The purity is given by

$$\begin{aligned} \text{Pu} &= \sum_{v'=0}^{N_v-1} \sum_{v''=0}^{N_v-1} p_{v'} p_{v''} e^{-\frac{1}{\delta\Omega^2}(\omega^{v'} - \omega^{v''})^2} \\ &\quad \times \cos^2\{(\omega^{v'} - \omega^{v''})\tau_x/2\}, \end{aligned} \quad (21)$$

meaning that the state of H_2^+ is pure when $(\omega^{v'} - \omega^{v''})\tau_x/2$ is equal to an integer multiple of π for any $v'-v''$ pair. This requirement is the same as the condition that τ_x coincides with the revival time of the vibrational wave packet T_{rev} , which is approximately 280 fs for the vibrational wave packet in the $1s\sigma_g$ state of H_2^+ . The evolutions of the purity and the von Neumann entropy are indeed both similar to the evolution of the vibrational wave packet as shown in Figs. 2(a) and 2(b). We assumed a pair of XUV Fourier limit pulses with a bandwidth of 2.25 eV and a center angular frequency of 21.8 eV, both of which were the same values adopted in Ref. [18], to calculate Pu and \mathbf{S} in these figures. We observe from Figs. 2(a) and 2(b) that Pu and \mathbf{S} are both modulated, mainly with a period of vibrational motion of ≈ 17 fs, and we also find that Pu is maximized and \mathbf{S} is minimized, when $\tau_x = 0$ and $\tau_x \simeq T_{\text{rev}}, 2T_{\text{rev}}$. Note that the maximum value of Pu does not reach unity and the minimum value of \mathbf{S} does not fall to zero because $\delta\Omega$ is large but finite.

III. TWO-PHOTON INTERACTION

A. General form of the state vector

We analyze the third term in Eq. (A20) in Appendix A to express the state vector involving the two-photon

excitation/ionization process defined as

$$|\Psi^{(2)}(\mathbf{R}; t)\rangle \equiv \left(\frac{1}{i\hbar}\right)^2 \int_{t_0}^t dt_1 \int_{t_0}^{t_1} dt_2 e^{\frac{\hat{H}(\mathbf{R})}{i\hbar}(t-t_1)} \hat{V}(t_1) e^{\frac{\hat{H}(\mathbf{R})}{i\hbar}(t_1-t_2)} \hat{V}(t_2) e^{\frac{\hat{H}(\mathbf{R})}{i\hbar}(t_2-t_0)} |\Psi(\mathbf{R}; t_0)\rangle. \quad (22)$$

We assume the initial state to be the ground vibrational state in the ground electronic state of a general molecule M , $|\Psi_g^0(\mathbf{R})\rangle$, and the final state to be the $e^- \otimes M^+$ system, $|\Psi_i^{(2)}(\mathbf{R}; t)\rangle$, which is proportional to the superposition of $|\Psi_\beta^{+v'}(\mathbf{R})\rangle |\psi_{c_\beta}(\omega_e)\rangle$ with respect to β , v' , and ω_e , as was adopted in the previous section. Placing the approximate resolution of identity expressed as Eq. (2) in front of $\hat{V}(t_1)$ and in front of $\hat{V}(t_2)$, the state vector is divided into two parts: $|\Psi_i^{(2)}(\mathbf{R}; t)\rangle = |\Psi_{i_0}^{(2)}(\mathbf{R}; t)\rangle + |\Psi_{i_+}^{(2)}(\mathbf{R}; t)\rangle$, where we respectively define the first and second terms on the right-hand side of this equation as

$$|\Psi_{i_0}^{(2)}(\mathbf{R}; t)\rangle \equiv -\frac{1}{\hbar^2} \int_{t_0}^t dt_1 \int_{t_0}^{t_1} dt_2 \int d^3M \mathbf{R}_1 \int d^3M \mathbf{R}_2 e^{\frac{\hat{H}(\mathbf{R})}{i\hbar}(t-t_1)} \times \hat{P}^+(\mathbf{R}, \mathbf{R}_1) \hat{V}(t_1) e^{\frac{\hat{H}(\mathbf{R}_1)}{i\hbar}(t_1-t_2)} \hat{P}(\mathbf{R}_1, \mathbf{R}_2) \hat{V}(t_2) e^{\frac{E_g^0}{i\hbar}(t_2-t_0)} |\Psi_g^0(\mathbf{R}_2)\rangle, \quad (23)$$

$$|\Psi_{i_+}^{(2)}(\mathbf{R}; t)\rangle \equiv -\frac{1}{\hbar^2} \int_{t_0}^t dt_1 \int_{t_0}^{t_1} dt_2 \int d^3M \mathbf{R}_1 \int d^3M \mathbf{R}_2 e^{\frac{\hat{H}(\mathbf{R})}{i\hbar}(t-t_1)} \times \hat{P}^+(\mathbf{R}, \mathbf{R}_1) \hat{V}(t_1) e^{\frac{\hat{H}(\mathbf{R}_1)}{i\hbar}(t_1-t_2)} \hat{P}^+(\mathbf{R}_1, \mathbf{R}_2) \hat{V}(t_2) e^{\frac{E_g^0}{i\hbar}(t_2-t_0)} |\Psi_g^0(\mathbf{R}_2)\rangle. \quad (24)$$

The state vector of $|\Psi_{i_0}^{(2)}(\mathbf{R}; t)\rangle$ in Eq. (23) coincides with the transition from the initial state to the excited states of the neutral molecule with one-photon absorption followed by ionization by the absorption of one more photon, while that of $|\Psi_{i_+}^{(2)}(\mathbf{R}; t)\rangle$ in Eq. (24) describes the two-photon ionization and transition via the ground and excited states of the molecular ion. Substituting Eqs. (A8) and (A17) into Eqs. (23) and (24), and respectively approximating $t \rightarrow \infty$ and $t_0 \rightarrow -\infty$ for the upper and lower limits in the time integrals, we can rewrite these formulas as follows:

$$|\Psi_{i_0}^{(2)}(\mathbf{R}; t)\rangle = -\frac{1}{\hbar^2} \sum_\gamma \sum_{v''} \int_0^\infty d\omega'_e |\Psi_\gamma^{+v''}(\mathbf{R})\rangle |\psi_{c_\gamma}(\omega'_e)\rangle e^{-i(\omega_\gamma^{+v''} + \omega'_e)t} e^{i\omega_g^0 t_0} \times \sum_\beta \sum_{v'} \mu_{\gamma\beta}^{+v''v'}(\omega'_e) \mu_{\beta g}^{v'} \int dt_1 \int dt_2 \theta(t_1 - t_2) E(t_1) E(t_2) e^{i(\omega_\gamma^{+v''} + \omega'_e - \omega_\beta^{v'})t_1} e^{i(\omega_\beta^{v'} - \omega_g^0)t_2}, \quad (25)$$

$$|\Psi_{i_+}^{(2)}(\mathbf{R}; t)\rangle = -\frac{1}{\hbar^2} \sum_\gamma \sum_{v''} \int_0^\infty d\omega'_e |\Psi_\gamma^{+v''}(\mathbf{R})\rangle |\psi_{c_\gamma}(\omega'_e)\rangle e^{-i(\omega_\gamma^{+v''} + \omega'_e)t} e^{i\omega_g^0 t_0} \times \sum_\beta \sum_{v'} \mu_{\gamma\beta}^{+v''+v'} \mu_{\beta g}^{+v'}(\omega'_e) \int dt_1 \int dt_2 \theta(t_1 - t_2) E(t_1) E(t_2) e^{i(\omega_\gamma^{+v''} - \omega_\beta^{+v'})t_1} e^{i(\omega_\beta^{+v'} + \omega'_e - \omega_g^0)t_2}, \quad (26)$$

where we neglect the energy transfer between the continuum electronic states, allowing us to apply the approximation

$$\int d^3M \mathbf{R} \langle \Psi_\gamma^{+v''}(\mathbf{R}) | \langle \psi_{c_\gamma}(\omega'_e) | \hat{\mu} | \psi_{c_\beta}(\omega'_e) \rangle | \Psi_\beta^{+v'}(\mathbf{R}) \rangle \simeq \delta(\omega'' - \omega'_e) \int d^3M \mathbf{R} \langle \Psi_\gamma^{+v''}(\mathbf{R}) | \hat{\mu}^+ | \Psi_\beta^{+v'}(\mathbf{R}) \rangle \equiv \delta(\omega'' - \omega'_e) \mu_{\gamma\beta}^{+v''+v'} \quad (27)$$

to obtain Eq. (26). We introduce the Heaviside step function $\theta(t)$ in Eqs. (25) and (26). The dipole moment $\mu_{\gamma\beta}^{+v''+v'}$ in Eq. (26) is regarded as the transition amplitude from the β -electronic and v' th nuclear state in a molecular ion (v' may be a continuum if the states of the molecular ion involve dissociation) to the γ -electronic and v'' th nuclear state in a molecular ion, while the dipole moment $\mu_{\gamma\beta}^{+v''v'}(\omega'_e)$ in Eq. (25) is the transition amplitude from the β -electronic and v' th nuclear state in the neutral molecule to the γ -electronic and v'' th nuclear state in the molecular ion accompanying the

continuum electron with a KE of $\hbar\omega'_e$. Other dipole moments have already been defined in Sec. II A.

B. Two-photon ionization/dissociation of the H_2 molecule

We can use Eqs. (25) and (26) to obtain the general form of the autocorrelation or cross-correlation function of the XUV pulse involving the molecular response, as already stated in Ref. [19]. We do not, however, give further details of the autocorrelation function in the main text of this paper to focus on the probing process of the vibrational wave packet in the $1s\sigma_g$ state of H_2^+ by the UV pulse irradiation providing the second photon, although we give a brief explanation in Appendix B. We consider only the process described using Eq. (26) because the probe is implemented via the excitation of the ground electronic state within a molecular ion generated by the ionization with the first photon.

To adjust the state vector $|\Psi_{i_+}^{(2)}(\mathbf{R}; t)\rangle$ to the state of the $e^- \otimes \text{H}_2^+$ system, we impose somewhat intentional approximations on Eq. (26). First, we include only the dipole moment

from the $1s\sigma_g$ state to the $2p\sigma_u$ state of H_2^+ and discard other dipole moments from the summation for the electronic states \sum_β and \sum_γ , because we expect the magnitude of the $1s\sigma_g \rightarrow 2p\sigma_u$ dipole moment to be much larger than those of other dipole moments from our past experimental results [20–22]. This approximation might contradict the fact that we actually observed H^+ fragments via the transition to the $2p\pi_u$ state when the probe was an XUV APT [22]. We also found the autocorrelation signal of the APT on the H^+ fragment with high KEs [23], which originated from the nonresonant contribution of the small dipole moments accumulated. Nev-

ertheless, we also know that the yield of the H^+ fragment via the $2p\sigma_u$ state by absorbing a UV photon was significantly larger than those through other dissociation pathways involving the absorption of an XUV photon. Thus, we simplify the situation by adopting the approximation mentioned above. As the $2p\sigma_u$ state is dissociative, we replace the quantum number v'' with κ'' to express the continuum variable, and the symbol $\sum_{v''}$ is reduced to the simple integral $\int_{\kappa_0}^{\infty} d\kappa''$, where $\hbar\kappa' \equiv \hbar\kappa'' - \hbar\kappa_0$ is the KER of the $2p\sigma_u$ state and $\hbar\kappa_0$ is the constant energy of the dissociation limit. Then, Eq. (26) is reduced to

$$|\Psi_{i_+}^{(2)}(\mathbf{R}; t)\rangle = -\frac{1}{\hbar^2} \int_0^\infty d\kappa' \int_0^\infty d\omega'_e |\Psi_{2p\sigma_u}^+(\mathbf{R}; \kappa' + \kappa_0)\rangle |\psi_c(\omega'_e)\rangle e^{-i(\kappa' + \kappa_0 + \omega'_e)t} \\ \times \sum_{v'} \mu_{2p\sigma_u}^{+v'}(\kappa') \mu_{1s\sigma_g}^{+v'}(\omega'_e) S(\kappa' + \kappa_0 - \omega^{+v'}, \omega^{+v'} + \omega'_e - \omega_g^0; \tau_x, \tau_u), \quad (28)$$

where we define the transition dipole moment from the ground electronic-vibrational state of H_2 to the v' th vibrational state in the $1s\sigma_g$ state of H_2^+ accompanying the continuum electron with a KE of $\hbar\omega'_e$ as $\mu_{1s\sigma_g}^{+v'}(\omega'_e)$ and that from the v' th vibrational state in the $1s\sigma_g$ state to the $2p\sigma_u$ state with a KER of $\hbar\kappa'$ as $\mu_{2p\sigma_u}^{+v'}(\kappa')$. Note that we express the energy of the $2p\sigma_u$ state as $\hbar(\kappa' + \kappa_0)$ so as to describe the KER as $\hbar\kappa'$. The constant phase factor $e^{i\omega_g^0 t_0}$ is omitted. We show the potential curves of the electronic states in Fig. 3 for easy understanding of the relation among the energies involved on the right-hand side of Eq. (28). The photon energies of the XUV and UV pulses are depicted as vertical arrows. The continuum energies of a photoelectron and the KER of the $H + H^+$ system are also similarly depicted.

We express the double time integration amplitude as $S(\Omega_1, \Omega_2; \tau_x, \tau_u)$ in Eq. (28), which is defined as

$$S(\Omega_1, \Omega_2; \tau_x, \tau_u) \equiv \int dt_1 \int dt_2 \theta(t_1 - t_2) E(t_1) E(t_2) e^{i\Omega_1 t_1} e^{i\Omega_2 t_2}. \quad (29)$$

We explicitly show the τ_x and τ_u delays of the electric fields described in Eq. (A19). The energy $\hbar\Omega_1 = \hbar\kappa' + \hbar\kappa_0 - \hbar\omega^{+v'}$ is the excitation energy in H_2^+ , and $\hbar\Omega_2 = \hbar\omega'_e + \hbar\omega^{+v'} - \hbar\omega_g^0$ coincides with the total energy required to generate a continuum electron with a KE of $\hbar\omega'_e$ by ionization.

Substituting Eq. (A19) into Eq. (29), we can rewrite S as $S = S_{ux} + S_{xu} + S_{uu} + S_{xx}$, where the amplitude S_{ux} is defined as the following time-ordered integration amplitude:

$$S_{ux}(\Omega_1, \Omega_2; \tau_x, \tau_u) \equiv \int dt_1 \int dt_2 \theta(t_1 - t_2) E_u(t_1 - \tau_u) E_x(t_2; \tau_x) e^{i\Omega_1 t_1} e^{i\Omega_2 t_2}. \quad (30)$$

Other terms are obtained by replacing $E_u(t_1 - \tau_u) E_x(t_2; \tau_x)$ with $E_x(t_1; \tau_x) E_u(t_2 - \tau_u)$, $E_u(t_1 - \tau_u) E_u(t_2 - \tau_u)$, and $E_x(t_1; \tau_x) E_x(t_2; \tau_x)$ in Eq. (30). We restrict ourselves to considering only the amplitude $S_{ux}(\Omega_1, \Omega_2; \tau_x, \tau_u)$ because this term mainly contributes to the double time integration amplitude under the resonant excitation condition from the $1s\sigma_g$ state to the $2p\sigma_u$ state upon the UV field irradiation, as shown later.

Using the Fourier representation of the Heaviside step function $\theta(t) = \int d\Omega \tilde{\theta}(\Omega) e^{-i\Omega t}$ (the coefficient $\frac{1}{2\pi}$ is omitted from the formula of the inverse FT defined in Sec. II A), we obtain the formula $S_{ux}(\Omega_1, \Omega_2; \tau_x, \tau_u) = \int d\Omega \tilde{\theta}(\Omega_1 - \Omega) \tilde{E}_u(\Omega) \tilde{E}_x(\Omega_1 + \Omega_2 - \Omega; \tau_x) e^{i\Omega_1 \tau_u} = \int d\Omega \tilde{\theta}(\Omega_1 - \Omega) \tilde{A}_u(\Omega - \omega_u) \tilde{A}_x(\Omega_1 + \Omega_2 - \Omega - \omega_x; \tau_x) e^{i\Omega_1 \tau_u}$, where we adopt the Fourier amplitudes of the field envelopes defined in Eqs. (5) and (6). Substituting the explicit form of $\tilde{\theta}(\Omega) = -\frac{1}{2i\pi} \mathcal{P} \frac{1}{\Omega} + \frac{1}{2} \delta(\Omega)$ into this equation, we have

$$S_{ux}(\Omega_1, \Omega_2; \tau_x, \tau_u) = -\frac{1}{2i\pi} \mathcal{P} \int d\Omega \frac{\tilde{A}_u(\Omega_1 - \omega_u - \Omega) \tilde{A}_x(\Omega_2 - \omega_x + \Omega; \tau_x) e^{-i\Omega \tau_u}}{\Omega} e^{i\Omega_1 \tau_u} \\ + \frac{1}{2} \tilde{A}_u(\Omega_1 - \omega_u) \tilde{A}_x(\Omega_2 - \omega_x; \tau_x) e^{i\Omega_1 \tau_u} \\ \equiv -\frac{1}{2i\pi} \mathcal{P} \int d\Omega f(\Omega) e^{i\Omega_1 \tau_u} + \frac{1}{2} \tilde{A}_u(\Omega_1 - \omega_u) \tilde{A}_x(\Omega_2 - \omega_x; \tau_x) e^{i\Omega_1 \tau_u}, \quad (31)$$

where the symbol \mathcal{P} denotes the principal value integral (PVI) of $f(\Omega)$. We examine the asymptotic behavior of the PVI by

assuming that $\tilde{A}_u(\Omega)$ and $\tilde{A}_x(\Omega)$ are modeled with a simple analytical form such as the n th power of the Lorentz function,

namely, $\tilde{A}_{u,x}(\Omega) \propto \{\frac{\Omega^2}{\delta\Omega_{u,x}^2} + 1\}^{-n}$. Although the temporal envelope may not be a realistic form, this model of the Fourier amplitude is convenient for qualitatively evaluating the PVI. The PVI of the Gaussian function with the analytical form is derived in Appendix B.

By replacing Ω with a complex variable z , we can implement a closed contour integral on the complex plane. When τ_u and $\tau_u - \tau_x$ are both positive and significantly larger than the pulse durations of both fields, $\delta\Omega_{u,x}^{-1}$, the contribution of the semicircle contour in the lower half of the complex plane approaches zero as its radius approaches infinity. A schematic of the contours relevant to the PVI estimation is shown in Fig. 10(b) in Appendix B. The closed contour is composed of the PVI on the real axis, the semicircle contour with an infinitesimal radius surrounding zero in the lower half of the complex plane, and the infinite-radius semicircle contour in the lower half of the complex plane, which are indicated as C_z^- , C_{ϵ^-} , and C_{R^-} in Fig. 10(b) in Appendix B, respectively.

As the contributions from the poles in the closed contour are proportional to $\tau_u^m e^{-\delta\Omega_{u,x}\tau_u}$, or $\tau_u^m e^{-\delta\Omega_{u,x}(\tau_u - \tau_x)}$, both of which are close to zero under the imposed condition, the value of the closed contour integral is approximately zero. At the same time, the contribution from the semicircle contour with the infinitesimal radius should be $i\pi$ times the residue at $z=0$ [$i\pi \text{Res}_{z=0}\{f(z)\}$] because the direction of the contour integral is counterclockwise. As a result, we obtain $\mathcal{P} \int d\Omega f(\Omega) + i\pi \text{Res}_{z=0}\{f(z)\} \simeq 0$, or $\mathcal{P} \int d\Omega f(\Omega) \simeq -i\pi \text{Res}_{z=0}\{f(z)\}$, for $\tau_u \gg \delta\Omega_{u,x}^{-1}$ and $\tau_u - \tau_x \gg \delta\Omega_{u,x}^{-1}$, which we call the large-delay condition. The situation is reversed when the delays are negative and $\tau_u \ll -\delta\Omega_{u,x}^{-1}$ and $\tau_u - \tau_x \ll -\delta\Omega_{u,x}^{-1}$. We have to choose the closed contour in the upper half of the complex plane, then we find that $\mathcal{P} \int d\Omega f(\Omega) \simeq i\pi \text{Res}_{z=0}\{f(z)\}$. We evaluate $\text{Res}_{z=0}\{f(z)\} = \tilde{A}_u(\Omega_1 - \omega_u)\tilde{A}_x(\Omega_2 - \omega_x; \tau_x)$ by assuming that $z=0$ is a simple pole of $f(z)$; thus, the resultant asymptotic form of the amplitude $S_{ux}(\Omega_1, \Omega_2; \tau_x, \tau_u)$ in Eq. (31) is estimated to be the following form:

$$S_{ux}(\Omega_1, \Omega_2; \tau_x, \tau_u) \simeq \begin{cases} \tilde{A}_u(\Omega_1 - \omega_u)\tilde{A}_x(\Omega_2 - \omega_x; \tau_x)e^{i\Omega_1\tau_u} & \text{for } \tau_u \gg \delta\Omega_{u,x}^{-1} \quad \text{and} \quad \tau_u - \tau_x \gg \delta\Omega_{u,x}^{-1} \\ 0 & \text{for } \tau_u \ll -\delta\Omega_{u,x}^{-1} \quad \text{and} \quad \tau_u - \tau_x \ll -\delta\Omega_{u,x}^{-1}. \end{cases} \quad (32)$$

Because the argument in \tilde{A}_u is equal to $\Omega_1 - \omega_u = \kappa' + \kappa_0 - \omega^{+v'} - \omega_u$, the carrier photon energy of the UV pulse must be nearly equal to the excitation energy from the $1s\sigma_g$ state to the $2p\sigma_u$ state in H_2^+ or, simply, the resonant excitation is mandatory to obtain a substantial magnitude of $S_{ux}(\Omega_1, \Omega_2; \tau_x, \tau_u)$. In addition, from the argument in \tilde{A}_x , the carrier photon energy of the XUV pulse must be larger than the ionization energy so as to realize $\Omega_2 - \omega_x = \omega'_e - \{\omega_x - (\omega^{+v'} - \omega_g^0)\} \simeq 0$ in the region $\omega'_e > 0$. These two requirements for the carrier photon energies of the UV and XUV pulses are natural and do not require consideration of the theoretical model in detail, but they are significant in obtaining a reasonable approximation of $S(\Omega_1, \Omega_2; \tau_x, \tau_u) \simeq S_{ux}(\Omega_1, \Omega_2; \tau_x, \tau_u)$ by neglecting S_{xu} , S_{uu} , and S_{xx} . The amplitude S_{xu} is obtained by interchanging t_1 and t_2 on the right-hand side of Eq. (30), which is equivalent to the exchange of Ω_1 and Ω_2 and the sign change of $\Omega \rightarrow -\Omega$ on the right-hand side of Eq. (31). Therefore, we find that S_{xu} is finite only in the region of negative τ_u and $\tau_u - \tau_x$ with large magnitudes and it contains the factor $\tilde{A}_u[\omega'_e - \{\omega_u - (\omega^{+v'} -$

$\omega_g^0)\}\tilde{A}_x(\kappa' + \kappa_0 - \omega^{+v'} - \omega_x; \tau_x)$. The carrier photon energy of the UV pulse is lower than the ionization energy, and thus $\omega'_e - \{\omega_u - (\omega^{+v'} - \omega_g^0)\}$ cannot become zero whenever ω'_e is positive. As a result, the magnitude of S_{xu} is negligibly small compared with that of S_{ux} . For the same reason, we can neglect the amplitude S_{uu} . The contribution of the amplitude S_{xx} cannot be neglected only for the reason mentioned above. Actually, we successfully measured the vibrational motion of an H_2^+ molecule by detecting the H^+ ions emerging upon XUV excitation in a past experiment [22]. However, this measurement was possible only when the intensity of the XUV pulse was sufficiently high. Thus, we impose the condition that the contribution of the amplitude S_{xx} is small compared with that of the amplitude S_{ux} due to the low intensity of the XUV pulse.

We rewrite the right-hand side of Eq. (28) by replacing S with S_{ux} and substituting Eq. (32) under the large-delay condition

$$|\Psi_{i+}^{(2)}(\mathbf{R}; t)\rangle = -\frac{1}{\hbar^2} \int_0^\infty dk' \int_0^\infty d\omega'_e |\Psi_{2p\sigma_u}^+(\mathbf{R}; \kappa' + \kappa_0)\rangle |\psi_c(\omega'_e)\rangle e^{-i(\kappa' + \kappa_0 + \omega'_e)t} \sum_{v'} \mu_{2p\sigma_u}^{+v'}(\kappa') \times \mu_{1s\sigma_g}^{+v'}(\omega'_e)\tilde{A}_u(\kappa' + \kappa_0 - \omega^{+v'} - \omega_u)\tilde{A}_x(\omega^{+v'} + \omega'_e - \omega_g^0 - \omega_x; \tau_x)e^{i(\kappa' + \kappa_0 - \omega^{+v'})\tau_u}. \quad (33)$$

We obtain the $\mathbf{R}'\text{-}\mathbf{R}''$ element of the second-order density matrix expressing the ionization and excitation process, $\hat{\rho}_{i+}^{(2)}(\mathbf{R}', \mathbf{R}''; t)$, as

$$\hat{\rho}_{i+}^{(2)}(\mathbf{R}', \mathbf{R}''; t) \propto |\Psi_{i+}^{(2)}(\mathbf{R}'; t)\rangle \langle \Psi_{i+}^{(2)}(\mathbf{R}''; t)|. \quad (34)$$

We normalize $\hat{\rho}_{i+}^{(2)}(\mathbf{R}', \mathbf{R}''; t)$ so as to satisfy

$$\text{Tr}\{\hat{\rho}_{i+}^{(2)}\} = \int d^3\mathbf{R} \hat{\rho}_{i+}^{(2)}(\mathbf{R}, \mathbf{R}; t) = |C_+|^2 \int d^3\mathbf{R} \langle \Psi_{i+}^{(2)}(\mathbf{R}; t) | \Psi_{i+}^{(2)}(\mathbf{R}; t) \rangle = 1 \quad (35)$$

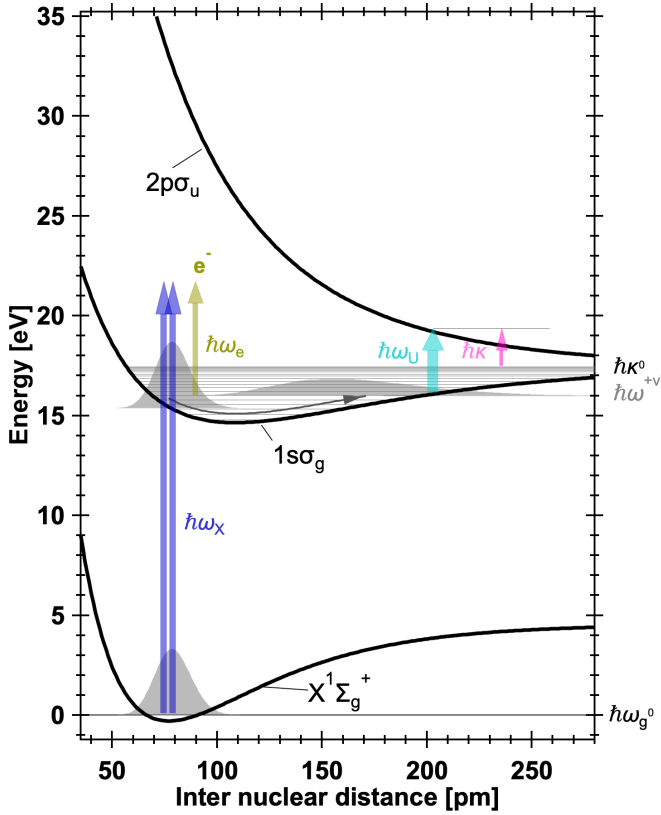


FIG. 3. Energy diagram related to Eq. (28). The potential energy curve of the $X^1\Sigma_g^+$ state in H_2 , and those of the $1s\sigma_g$ and $2p\sigma_u$ states in H_2^+ , are shown as labeled black curves. The photon energy of the XUV pulse pair is indicated as the length of blue-violet vertical arrows labeled $\hbar\omega_x$, and that of the UV pulse is also indicated as the length of the cyan vertical arrow labeled $\hbar\omega_u$. The length of the gold arrow labeled $\hbar\omega_e$ and that of the pink arrow labeled $\hbar\kappa$ are equivalent to the energy of the continuum electron and the KER of the $H + H^+$ system, respectively. The energy level of the ground vibrational state in the $X^1\Sigma_g^+$ state of H_2 is labeled $\hbar\omega_g^0$ on the right axis. The energy levels of the v' th vibrational state and the dissociation limit in H_2^+ are also labeled $\hbar\omega^{+v'}$ and $\hbar\kappa^0$ on the right axis, respectively. The gray shaded area on the $X^1\Sigma_g^+$ potential curve is the intensity profile (square) of the ground vibrational function in the $X^1\Sigma_g^+$ state; immediately above this, the intensity profile of the wave packet projected onto the $1s\sigma_g$ potential curve is depicted in a similar manner. The wave packet on the $1s\sigma_g$ potential curve evolving after ≈ 10 fs is depicted as the gray shaded area at an internuclear distance of ≈ 160 pm.

when we need to evaluate the purity or von Neumann entropy of the reduced density matrix.

C. Joint measurement of the KE of an electron and the KER of a $H + H^+$ system

We confirm that the state vector $|\Psi_{i+}^{(2)}(\mathbf{R}; t)\rangle$ in Eq. (33) or the density matrix $\hat{\rho}_{i+}^{(2)}(\mathbf{R}', \mathbf{R}''; t)$ in Eq. (34) is appropriate by verifying that the joint probability of simultaneously detecting an electron with a KE of $\hbar\omega_e$ and a proton with a KE of $\hbar\kappa/2$ calculated from $|\Psi_{i+}^{(2)}(\mathbf{R}; t)\rangle$ or $\hat{\rho}_{i+}^{(2)}(\mathbf{R}', \mathbf{R}''; t)$ is consistent with that demonstrated in Ref. [4]. An observable for this joint measurement $\hat{O}(\mathbf{R}, \mathbf{R}'; \kappa, \omega_e)$ may be the projection operator

to the state $|\Psi_{2p\sigma_u}^+(\mathbf{R}; \kappa + \kappa_0)\rangle |\psi_c(\omega_e)\rangle e^{-i(\kappa + \kappa_0 + \omega_e)t}$ when we assume the projective measurement, and thus we define

$$\hat{O}(\mathbf{R}, \mathbf{R}'; \kappa, \omega_e) \equiv |\Psi_{2p\sigma_u}^+(\mathbf{R}; \kappa + \kappa_0)\rangle |\psi_c(\omega_e)\rangle \langle \psi_c(\omega_e)| \times \langle \Psi_{2p\sigma_u}^+(\mathbf{R}'; \kappa + \kappa_0)| \quad (36)$$

as the observable. The JES $\mathbb{P}(\kappa, \omega_e)$ is proportional to $\text{Tr}\{\hat{O}(\kappa, \omega_e)\hat{\rho}_{i+}^{(2)}(t)\}$, which is identical to the following equation:

$$\begin{aligned} \mathbb{P}(\kappa, \omega_e) &\propto \int d^3\mathbf{R} \int d^3\mathbf{R}' \langle \psi_c(\omega_e) | \langle \Psi_{2p\sigma_u}^+(\mathbf{R}'; \kappa + \kappa_0) | \hat{\rho}_{i+}^{(2)} \\ &\quad \times (\mathbf{R}', \mathbf{R}; t) | \Psi_{2p\sigma_u}^+(\mathbf{R}; \kappa + \kappa_0) | \psi_c(\omega_e) \rangle \\ &= \left| \int d^3\mathbf{R} \langle \psi_c(\omega_e) | \langle \Psi_{2p\sigma_u}^+(\mathbf{R}'; \kappa + \kappa_0) | \Psi_{i+}^{(2)}(\mathbf{R}; t) \right|^2 \\ &\propto \left| \sum_{v'} \mu_{2p\sigma_u}^{+v'}(\kappa) \mu_{1s\sigma_g}^{+v'}(\omega_e) \tilde{A}_u(\kappa + \kappa_0 - \omega^{+v'} - \omega_u) \tilde{A}_x \right. \\ &\quad \left. \times (\omega^{+v'} + \omega_e - \omega_g^0 - \omega_x; \tau_x) e^{-i\omega^{+v'}\tau_u} \right|^2, \quad (37) \end{aligned}$$

where we have inserted Eq. (33) into the second line to obtain the last line in Eq. (37). The overall phase factor $e^{-i(\kappa + \kappa_0 + \omega_e)t} e^{i\kappa\tau_u}$ does not influence the joint probability; thus, $\mathbb{P}(\kappa, \omega_e)$ in Eq. (37) is independent of the present time t . We apply the approximation in Eq. (13) to $\mu_{1s\sigma_g}^{+v'}(\omega_e) \simeq \mu^{+v'}$, which is independent of ω_e . The transition dipole moment of $\mu_{2p\sigma_u}^{+v'}(\kappa)$ is obtained as follows. Substituting $\gamma = 2p\sigma_u$, $+v'' = \kappa$, and $\beta = 1s\sigma_g$ into Eq. (27), we find

$$\begin{aligned} \mu_{2p\sigma_u}^{+v'}(\kappa) &= \int d^3\mathbf{R} \langle \Psi_{2p\sigma_u}(\kappa + \kappa_0; \mathbf{R}) | \hat{\mu}^+ | \Psi_{1s\sigma_g}^+(\mathbf{R}) \rangle \\ &= \int d^3\mathbf{R} \phi_{2p\sigma_u}^*(\kappa; \mathbf{R}) \phi_{1s\sigma_g}^{+v'}(\mathbf{R}) \langle \psi_{e_{2p\sigma_u}}^+(\mathbf{R}) | \hat{\mu}^+ | \psi_{e_{1s\sigma_g}}^+(\mathbf{R}) \rangle, \quad (38) \end{aligned}$$

where $\phi_{2p\sigma_u}(\kappa; \mathbf{R})$ is the dissociative nuclear wave function in the $2p\sigma_u$ state. We also approximate the electronic dipole moment $\langle \psi_{e_{2p\sigma_u}}^+(\mathbf{R}) | \hat{\mu}^+ | \psi_{e_{1s\sigma_g}}^+(\mathbf{R}) \rangle$ as proportional to $|\mathbf{R}|$ in the following calculations. The Fourier amplitude of the envelope of the XUV pulse pair is described as $\tilde{A}_x(\omega^{+v'} + \omega_e - \omega_g^0 - \omega_x; \tau_x) = \tilde{A}_x[\omega_e - \{\omega_x - (\omega^{+v'} - \omega_g^0)\}] \{1 + e^{i(\omega_e + \omega^{+v'} - \omega_g^0)\tau_x}\}$.

Substituting the Fourier amplitudes of the XUV pulse pair and the UV pulse into Eq. (37), we can obtain the joint energy spectrum $\mathbb{P}(\kappa, \omega_e)$ at a delay between the two XUV pulses of τ_x and a delay of the UV pulse from the first XUV pulse of τ_u . In accordance with Ref. [4], we adopt the form of the $\cos^2(\frac{t}{T})$ function as temporal amplitude envelopes of the XUV pulse pair and the UV pulse with full width at half maximum pulse durations of 690 as and 2.4 fs of the intensity envelope, δt_{FWHM} , respectively, where T is proportional to δt_{FWHM} , $T = \frac{\delta t_{\text{FWHM}}}{2\nu}$, and $\nu = \cos^{-1}(2^{-\frac{1}{4}})$. The carrier photon energy of the XUV pulse pair $\hbar\omega_x$ and that of the UV pulse $\hbar\omega_u$ are determined to be 21.76 and 3.1 eV, respectively.

We show the resultant JES, $\mathbb{P}(\kappa, \omega_e)$, of finding an electron with a KE of $\hbar\omega_e$ and a $H + H^+$ system with a KER of $\hbar\kappa$ at $\tau_x = 12.1$ fs and $\tau_u = 242$ fs in Fig. 4(a). In this figure, the photoelectron spectra in the entire KER spectral range

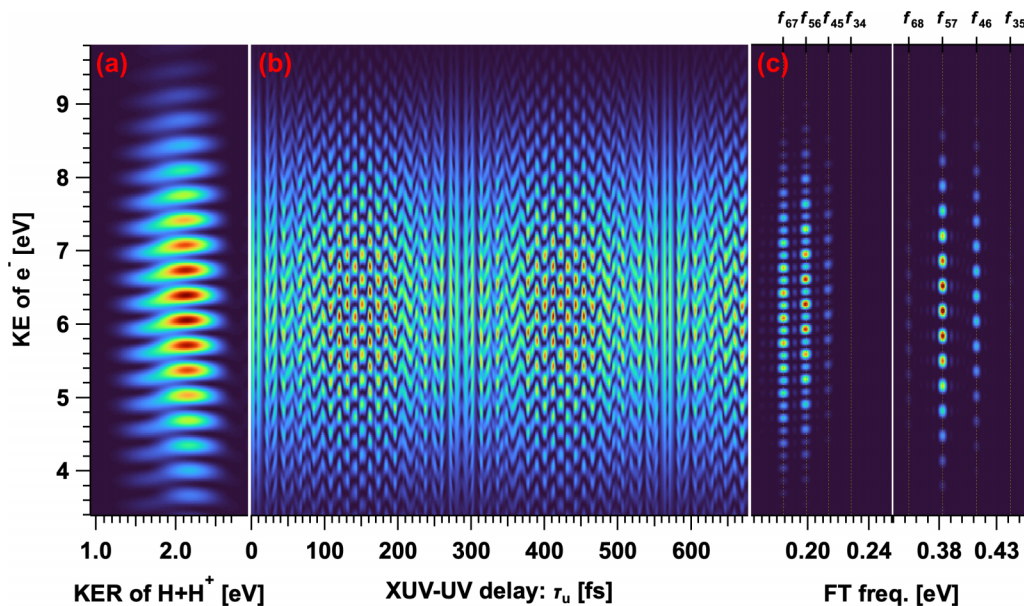


FIG. 4. (a) JES, $\mathbb{P}(\kappa, \omega_e)$, of finding an electron with a KE of $\hbar\omega_e$ and a $\text{H} + \text{H}^+$ system with a KER of $\hbar\kappa$ at $\tau_x = 12.1$ fs and $\tau_u = 242$ fs. (b) Evolution of the KE spectrum of an electron upon scanning τ_u jointly measured with a $\text{H} + \text{H}^+$ system with a KER of 1.8 eV. (c) Magnitude square of the FT of the joint KE spectrogram shown in Fig. 4(b). Magnified views in the Fourier frequency ranges of [0.163 eV, 0.255 eV] and [0.340 eV, 0.463 eV] are exhibited. The difference frequencies between the adjacent vibrational states and those between the next adjacent vibrational states are indicated as labels of f_{vw} above the ticks on the top axis and the grids with dotted lines.

of the $\text{H} + \text{H}^+$ system exhibit modulation with a period of 0.34 eV, which is equivalent to $\hbar\tau_x^{-1}$, and it presents a visible feature similar to a trilobite's back in the $\hbar\omega_e$ and $\hbar\kappa$ ranges of Fig. 4(a). These characteristics are in good agreement with those appearing in Fig. 1(a) in Ref. [4]. Note that the minima and maxima of the $\hbar\omega_e$ and $\hbar\kappa$ ranges of Fig. 4(a) coincide with those of Fig. 1(a) in Ref. [4], even though the units are different.

We also show the evolution of the joint KE spectrum of electrons at $\tau_x = 12.1$ fs upon changing τ_u when $\hbar\kappa$ is set to 1.8 eV in Fig. 4(b). Temporal modulations with a period of approximately 21 fs are clearly observed in this figure, while the peak KE positions of the modulations linearly shift with respect to the delay τ_u , resulting in a fishnetlike structure. We verify that the temporal modulation emerges from the vibrational wave packet of H_2^+ by FT of the delay-joint KE spectrogram (DJKS) in Fig. 4(b). The magnitude square of the FT spectrogram indeed exhibits discrete peaks located at the difference frequencies between the adjacent vibrational states in the left panel of Fig. 4(c) and those between the next adjacent vibrational states in the right panel of the same figure.

The specific characteristics demonstrated in Figs. 4(b) and 4(c) are the same as those shown in Figs. 1(b) and 1(c) in Ref. [4], and thus we conclude that our analytical model of the state vector described as Eq. (33) is a reasonably good approximate solution of the TDSE that reproduces the composite system consisting of a continuum electron and a $\text{H} + \text{H}^+$ system.

By virtue of the analytical form in Eq. (37), we expect that the computational cost of calculating the DJKS will be reasonably low compared with that required for the numerical integration of the TDSE, and thus we can calculate

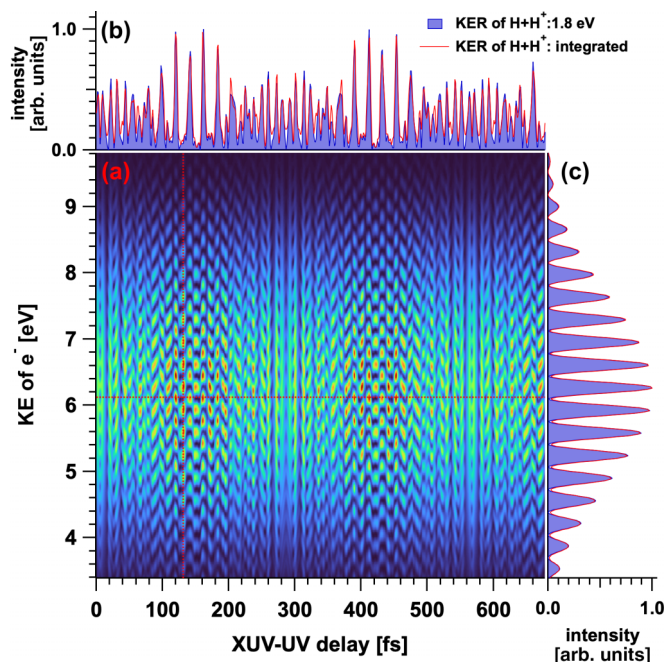


FIG. 5. (a) DJKS of an electron obtained by integrating DJKSs with KERs from 1.14 to 2.86 eV with an increment of 0.02 eV. (b) (Red curve) Line profile of the DJKS shown in (a) at an electron KE of 6.18 eV, the position of which is indicated as a red dotted horizontal line in (a), and (blue curve with shaded area) line profile of the DJKS shown in Fig. 4(b). (c) (Red curve) Line profile of the DJKS shown in (a) at a delay of 131 fs, the position of which is indicated as a red dotted vertical line in (a), and (blue curve with shaded area) line profile of the DJKS shown in Fig. 4(b).

multiple DJKSs under different conditions within a few minutes.

Taking advantage of the low computational cost, we accumulate DJKSs by changing the KER of the $H + H^+$ system to find the resolution required for the actual KER measurement. The resultant DJKS is shown in Fig. 5(a). We calculated 87 DJKSs in the KER range from 1.14 to 2.86 eV with an increment of 0.02 eV, in which the visible JES is involved as shown in Fig. 4(a), and added all the DJKSs to obtain the DJKS in this figure. We cannot find a notable difference between the DJKS shown in Fig. 4(b) and that shown in Fig. 5(a). The similarity of the two spectrograms is also confirmed by comparing their line profiles at a specific electron KE and a specific delay of the UV pulse. We show the profile of the joint probability of detecting an electron with a KE of 6.18 eV at a KER of 1.8 eV upon changing the delay of the

UV pulse as the blue curve with a shaded area in Fig. 5(b), which is very similar to that obtained by integrating the KER, shown as the red curve in the same figure. The KE spectral profile at a delay of 131 fs with a KER of 1.8 eV, shown as the blue curve with a shaded area in Fig. 5(c), is also almost identical to that with an integrated KER. Therefore, it is reasonable to conclude that we do not need to resolve the KER of the $H + H^+$ system, and that we only need to detect an H^+ ion in coincidence with a KE-resolved electron to acquire the DJKS. This is advantageous for designing an actual ion spectrometer used in the experiment because it must only distinguish the mass/charge ratio of the fragment ion.

The analytical form of the JES in Eq. (37) is also beneficial for finding the reason why the fishnetlike structure appears in the DJKS spectrogram. We rewrite Eq. (37) as

$$\begin{aligned} \mathbb{P}(\kappa, \omega_e) &\propto \sum_{v'v''} q^{v'} q^{*v''} e^{-i(\omega^{+v'} - \omega^{+v''})\tau_u} \{1 + e^{i(\omega_e + \omega^{+v'} - \omega_g^0)\tau_x}\} \{1 + e^{-i(\omega_e + \omega^{+v''} - \omega_g^0)\tau_x}\} \\ &= 2 \sum_{v'} |q^{v'}|^2 [1 + \cos\{(\omega_e + \omega^{+v'} - \omega_g^0)\tau_x\}] + 8 \sum_{v' > v''} |q^{v'} q^{*v''}| \cos\left(\Delta\omega^{+v'v''}\tau_u - \Delta\omega^{+v'v''}\frac{\tau_x}{2} - \Delta\phi^{v'v''}\right) \\ &\quad \times \cos\left\{(\omega_e + \omega^{+v'} - \omega_g^0)\frac{\tau_x}{2}\right\} \cos\left\{(\omega_e + \omega^{+v''} - \omega_g^0)\frac{\tau_x}{2} - \Delta\omega^{+v'v''}\frac{\tau_x}{2}\right\}, \end{aligned} \quad (39)$$

where we define $q^{v'} \equiv \mu_{2p\sigma_u}^{+v'}(\kappa)\mu_{1s\sigma_g}^{+v'}(\omega_e)\tilde{A}_u(\kappa - \{\omega_u + \omega^{+v'} - \kappa_0\})\tilde{A}_x[\omega_e - \{\omega_x - (\omega^{+v'} - \omega_g^0)\}]$, $\Delta\omega^{+v'v''} \equiv \omega^{+v'} - \omega^{+v''}$, and $\Delta\phi^{v'v''} \equiv \arg q^{v'} - \arg q^{v''}$.

We restrict ourselves to considering the $\mathbb{P}(\kappa, \omega_e)$ originating from only two vibrational states with vibrational numbers of $v' = 5$ and $v'' = 6$ because the most pronounced vibrational frequency in the DJKS spectrogram is f_{56} as shown in Fig. 4(c). We also assume that q^5 is approximately the same as q^6 and described as the real number q . Then, the JES $\mathbb{P}(\kappa, \omega_e)$ in Eq. (39) may be simplified to

$$\begin{aligned} \mathbb{P}(\kappa, \omega_e) &\sim 2q^2[2 + \cos(\tau_x\omega_e + \phi_X) + \cos(\tau_x\omega_e + \phi_X - \Delta\omega^{+56}\tau_x)] \\ &\quad + 8q^2 \cos\left(\Delta\omega^{+56}\tau_u - \Delta\omega^{+56}\frac{\tau_x}{2}\right) \cos\left(\frac{\tau_x}{2}\omega_e + \frac{\phi_X}{2}\right) \cos\left(\frac{\tau_x}{2}\omega_e + \frac{\phi_X}{2} - \Delta\omega^{+56}\frac{\tau_x}{2}\right), \end{aligned} \quad (40)$$

where we define $\phi_X \equiv \tau_x(\omega^{+5} - \omega_g^0)$. The first three terms in the square brackets in Eq. (40) express an electron spectrum exhibiting the interference of two sinusoidal functions with the same period τ_x and a phase difference of $\Delta\omega^{+56}\tau_x$, which is independent of the delay of the UV pulse τ_u . The last term in Eq. (40) specifies the evolution of the electron spectrum upon changing τ_u . We examine how the characteristic of the modulation in the DJKS spectrogram is altered by adopting special values of τ_x . First, we assume τ_x to be approximately equal to $\pi/\Delta\omega^{+56} \approx 10$ fs, namely $\Delta\omega^{+56}\tau_x \approx \pi$. The sinusoidal modulations in the square brackets are canceled out and the DJKS in Eq. (40) is reduced to the simple formula

$$\mathbb{P}(\kappa, \omega_e) \sim 4q^2\{1 + \sin(\Delta\omega^{+56}\tau_u)\sin(\tau_x\omega_e + \phi_X)\}. \quad (41)$$

We notice from Eq. (41) that the amplitude of the spectral interference fringes is modulated in accordance with $\sin(\Delta\omega^{+56}\tau_u)$, and thus the phases of the spectral modulation at $\Delta\omega^{+56}\tau_u = (2n - 1)\pi$, ($n = 1, 2, \dots$), where the visibility of the spectral interference fringes is maximized, are flipped by π compared with the phases at $\Delta\omega^{+56}\tau_u = 2n\pi$, where the visibility of the spectral interference fringes is also max-

imized. This characteristic of the DJKS can be clearly seen in Figs. 4(b) and 5(a), and it is the origin of the fishnetlike structure, although τ_x slightly deviates from 10 fs.

The characteristic of the DJKS is changed by fixing $\Delta\omega^{+56}\tau_x \approx 2\pi$ ($\tau_x \approx \pi/\Delta\omega^{+56} \approx 20$ fs). The DJKS in Eq. (40) is transformed to

$$\mathbb{P}(\kappa, \omega_e) \sim 4q^2\{1 + \cos(\Delta\omega^{+56}\tau_u)\}\{1 + \cos(\tau_x\omega_e + \phi_X)\}. \quad (42)$$

The spectral interference fringes described as $1 + \cos(\tau_x\omega_e + \phi_X)$ are only altered in their magnitude upon changing τ_u and do not exhibit the phase flip of the fringes.

We confirmed these characteristics at $\tau_x \approx 10$ and 20 fs by calculating DJKSs in accordance with Eq. (37), as shown in Figs. 6(a) and 6(b). We accumulated DJKSs in the KER region between 1.14 and 2.86 eV and substituted 10.3 fs for τ_x to obtain Fig. 6(a) and 20.6 fs for τ_x to obtain Fig. 6(b), respectively. We can again observe a fishnetlike structure in Fig. 6(a) and confirm that this structure originates from the π phase shift of the interference fringes of the joint KE spectral

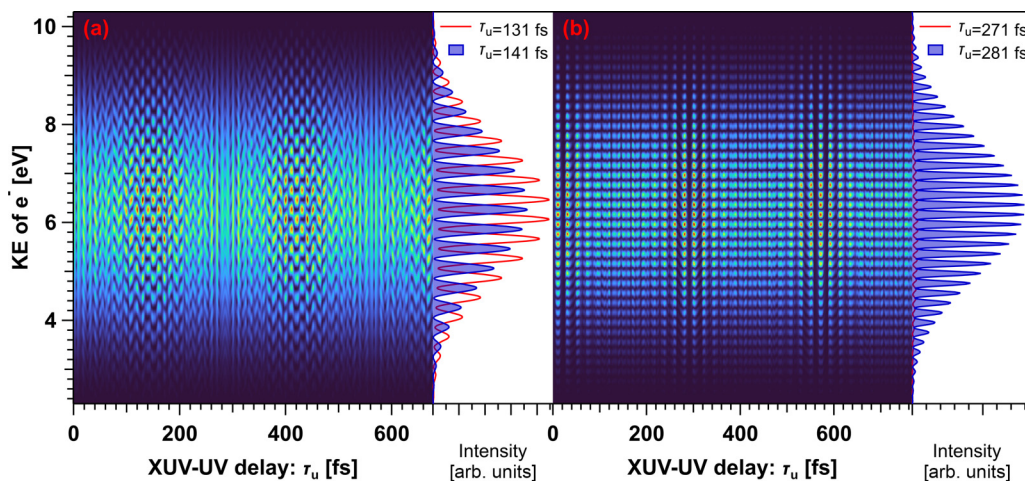


FIG. 6. DJKSs of the electron obtained by integrating DJKSs with KERs from 1.14 to 2.86 eV with an increment of 0.02 eV. (a) DJKS when 10.3 fs is substituted into τ_x , which is the delay between the two XUV pulses. The joint KE spectral profiles of the electron at $\tau_u = 131$ and 141 fs are depicted as a red curve and a blue curve with a shaded area in the right panel, respectively. (b) DJKS when 20.6 fs is substituted into τ_x . The joint KE spectral profiles of the electron at $\tau_u = 271$ and 281 fs are depicted as a red curve and a blue curve with a shaded area in the right panel, respectively.

profile upon an increment of τ_u of $\frac{\pi}{\Delta\omega^{+56}} \approx 10$ fs, shown as the red curve and the blue curve with a shaded area in the right panel of this figure. In contrast, in Fig. 6(b), each peak of the joint KE spectral profile is modulated at the same time in accordance with the advance of τ_u without changing the phase of the fringes. Actually, the joint KE spectral profile at $\tau_u = 271$ fs almost vanishes in the entire KE region, while that with interference fringes fully emerges at $\tau_u = 281$ fs, respectively, shown as the red curve and the blue curve with a shaded area in the right panel of this figure. Thus, we conclude that the simplified form of $\mathcal{P}(\kappa, \omega_e)$ in Eq. (40) is feasible for analyzing the periodicity and phase in the spectral modulations in DJKS spectrograms.

The visibility of the periodic modulation is maximized around $\tau_u \approx 140$ fs in Fig. 6(a), and around $\tau_u \approx 280$ fs in Fig. 6(b). The period of the visibility enhancement is ≈ 280 fs in both figures. These features cannot emerge from the simplified form of $\mathcal{P}(\kappa, \omega_e)$ in Eq. (40) because they are related to the anharmonicity of the vibrational energies, and thus the periodic modulations originating from $\Delta\omega^{+v'v'+1}$ other than $\Delta\omega^{+56}$ must be considered. Actually, the vibrational wave packet at the time around an integer multiple of the revival time T_{rev} is localized if the vibrational wave packet is created by the irradiation of a single XUV pulse, and thus the vibrational wave packet should be initially localized. This situation is similar to that applied to calculate the DJKS spectrogram in Fig. 6(b). The second XUV pulse is irradiated around the time when the vibrational wave packet created with the first XUV pulse returns to the inner turning point only after the one

round trip of the vibrational wave packet; thus, the vibrational wave packet is not significantly delocalized. Then the first quasilocalized vibrational wave packet is synthesized with the localized vibrational wave packet created with the second XUV pulse at the inner turning point. Therefore, the synthesized vibrational wave packet evolves in a similar manner to the first vibrational wave packet, resulting in enhanced visibility at every T_{rev} owing to the localization of the vibrational wave packet at every T_{rev} .

In contrast to the condition of the synthesized vibrational wave packet mentioned above, the first vibrational wave packet should be located around the outer turning point when the second XUV pulse is irradiated at $\tau_x \approx 10$ fs and the second vibrational wave packet is created at the inner turning point. The resultant synthesized vibrational wave packet is similar to the single vibrational wave packet that evolves after time $\frac{T_{\text{rev}}}{2}$. Therefore, the first enhancement of the visibility of the fringes in the DJKS spectrogram takes place around $\tau_u \sim \frac{T_{\text{rev}}}{2}$, as shown in Fig. 6(a), due to the localization of the synthesized vibrational wave packet.

D. Degrees of entanglement after UV pulse irradiation

Because the density matrix of the system involving the interaction with the UV pulse, $\hat{\rho}_{i+}^{(2)}(\mathbf{R}', \mathbf{R}''; t)$, is described by Eqs. (33) and (34), the $\kappa\kappa'$ element of the reduced density matrix of the H + H⁺ system, $\rho_{\text{ion}}^{(2)}(\kappa, \kappa'; \tau_x, \tau_u)$, is given by the following form:

$$\begin{aligned} \rho_{\text{ion}}^{(2)}(\kappa, \kappa'; \tau_x, \tau_u) &\propto \int_0^\infty d\omega_e \int d^3\mathbf{R} \int d^3\mathbf{R}' \langle \Psi_{2p\sigma_u}^+(\mathbf{R}; \kappa + \kappa_0) | \langle \psi_c(\omega_e) | \hat{\rho}_{i+}^{(2)}(\mathbf{R}, \mathbf{R}'; t) | \psi_c(\omega_e) \rangle | \Psi_{2p\sigma_u}^+(\mathbf{R}'; \kappa' + \kappa_0) \rangle \\ &\propto \sum_{v'v''} M_{v'}(\kappa; \tau_u) \rho_{\text{ion}_{v'v''}}^{(1)}(\tau_x) M_{v''}^*(\kappa'; \tau_u), \end{aligned} \quad (43)$$

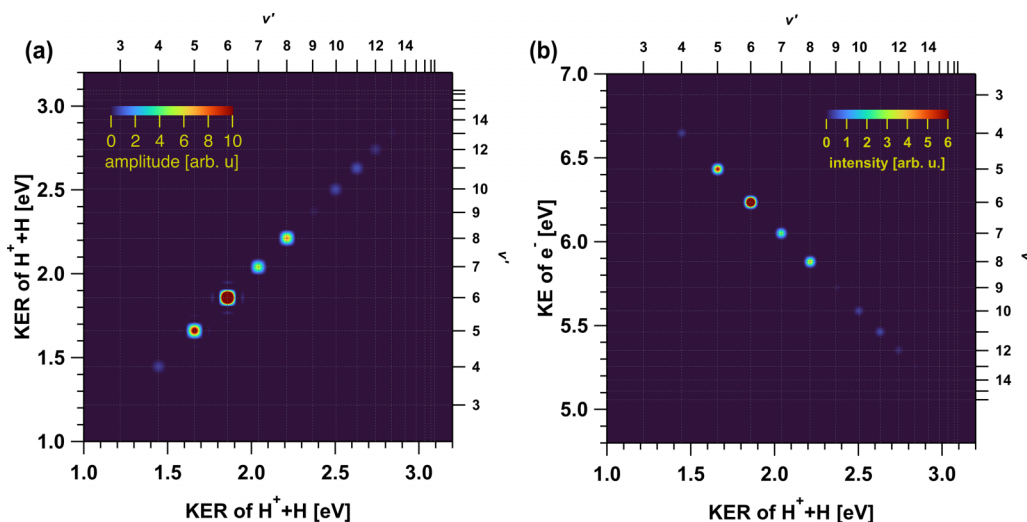


FIG. 7. (a) Real part of the reduced density matrix of the $2p\sigma_u$ state of the $\text{H} + \text{H}^+$ system $\rho_{\text{ion}}^{(2)}(\kappa, \kappa'; \tau_x = 0, \tau_u)$ calculated using Eq. (43). The bandwidths of the single XUV pulse and the UV probe pulse are both assumed to be 38 meV, which is smaller than the energy difference between the $v' + 1$ th and v' th ($v' \leq 14$) vibrational states in H_2^+ . Each tick of the v' th vibrational number at each KER position equivalent to $\hbar(\omega_u + \omega^{+v'} - \kappa_0)$ is indicated on the top and right axes. The color scale at the peak of $(v', v') = (6, 6)$ is intentionally saturated to enhance the weak amplitudes of other peaks. (b) JES, $\mathbb{P}(\kappa, \omega_e)$, of finding an electron with a KE of $\hbar\omega_e$ and a $\text{H} + \text{H}^+$ system with a KER of $\hbar\kappa$. Each tick of the v' th vibrational number at each KER position equivalent to $\hbar(\omega_u + \omega^{+v'} - \kappa_0)$ is indicated on the top axis. The position of a tick indicating the v' th vibrational number on the right axis coincides with $\hbar\{\omega_x - (\omega^{+v'} - \omega_g^0)\}$.

where $\rho_{\text{ion}_{v'v''}}^{(1)}(\tau_x)$ is given by Eq. (9) and $M_{v'}(\kappa; \tau_u)$ is defined as

$$M_{v'}(\kappa; \tau_u) \equiv \mu_{2p\sigma_u}^{+v'}(\kappa) \tilde{A}_u(\kappa + \kappa_0 - \omega^{+v'} - \omega_u) e^{-i\omega^{+v'}\tau_u}. \quad (44)$$

The purity or the von Neumann entropy of $\rho_{\text{ion}}^{(2)}(\kappa, \kappa'; \tau_x, \tau_u)$ indicates the degree of entanglement between the state of a continuum electron and the $2p\sigma_u$ state of a $\text{H} + \text{H}^+$ system.

We first examine a trivial example of entanglement by imposing a single narrow-bandwidth XUV field to diagonalize $\rho_{\text{ion}_{v'v''}}^{(1)}(\tau_x = 0)$, as was given by Eq. (19), and also imposing a narrow-bandwidth UV field, the Fourier amplitude of which, $\tilde{A}_u(\Omega - \omega_u)$, may be approximated as $\delta\omega \tilde{A}_{u0} \delta(\Omega - \omega_u)$. Then, the reduced density matrix can be simplified to

$$\rho_{\text{ion}}^{(2)}(\kappa, \kappa'; \tau_x = 0, \tau_u) \propto \delta(\kappa - \kappa') \sum_{v'} |\mu_{2p\sigma_u}^{+v'}(\kappa)|^2 p_{v'} \delta(\kappa - \kappa_{v'}), \quad (45)$$

where $\kappa_{v'}$ is defined as $\kappa_{v'} \equiv \omega_u + \omega^{+v'} - \kappa_0$. The reduced density matrix is τ_u independent, is diagonal, and exhibits discrete peaks at $\kappa = \kappa_{v'}$, as shown in Fig. 7(a), even though $\rho_{\text{ion}}^{(2)}(\kappa, \kappa'; \tau_x = 0, \tau_u)$ in this figure is calculated by assuming a finite (but narrow) bandwidth of the XUV and UV pulses. Therefore, we can determine that a continuum electron and a $\text{H} + \text{H}^+$ system are entangled after the irradiation of the UV pulse. The purity and the von Neumann entropy are estimated to be 0.385 and 1.87, respectively. In fact, the JES, $\mathbb{P}(\kappa, \omega_e)$, shown in Fig. 7(b) clearly exhibits discrete diagonal peaks, which approximately map the states of an $\text{H} + \text{H}^+$ system onto the state of a continuum electron. When we find an electron with a KE of 6.4 eV, we can determine the KER

of a $\text{H} + \text{H}^+$ system departing from the detected electron to be 1.66 eV without directly measuring the KER. When we apply the attosecond XUV pulse pair for photoionization and the few-femtosecond UV pulse for dissociation, as was adopted to calculate the JES in Fig. 4(a), the characteristic of the reduced density matrix drastically changes. We show the purity Pu and von Neumann entropy S of the reduced density matrix, $\rho_{\text{ion}}^{(2)}(\kappa, \kappa'; \tau_x, \tau_u)$, upon changing the delay of the UV probe pulse τ_u as a black solid curve with shaded areas in Figs. 8(a) and 8(b), respectively. We adopted a delay τ_x of zero between the XUV pulses to calculate these quantities. We also chose the delay times between the XUV pulses of 280.6 and 561.4 fs, where the von Neumann entropy of the reduced density matrix exhibits a local maximum and a local minimum, respectively, only after the irradiation of the XUV pulse pair, shown as the arrowed tags in Fig. 2(b). The resultant purities and von Neumann entropies of the reduced density matrices are depicted as the green solid curve and violet solid curve in Figs. 8(a) and 8(b), respectively.

We find that the purity and von Neumann entropy for $\tau_x = 0$ fs (black solid curve with shaded areas) are similar to those for $\tau_x = 561.4$ fs (violet solid curve). This is because the vibrational wave packet created upon the irradiation of the second XUV pulse is spatially and coherently superposed with the wave packet revived and localized around the inner turning point after the delay time of 561.4 fs from the birth of the wave packet upon the irradiation of the first XUV pulse. Readers are reminded that the approximated formula of the state vector given by Eq. (33) is valid only under the condition that $\tau_u - \tau_x$ is much larger than the pulse durations of the XUV and UV pulses, and thus we do not expect the purity and von Neumann entropy in the region of $\tau_u - \tau_x \lesssim 10$ fs to be correct.

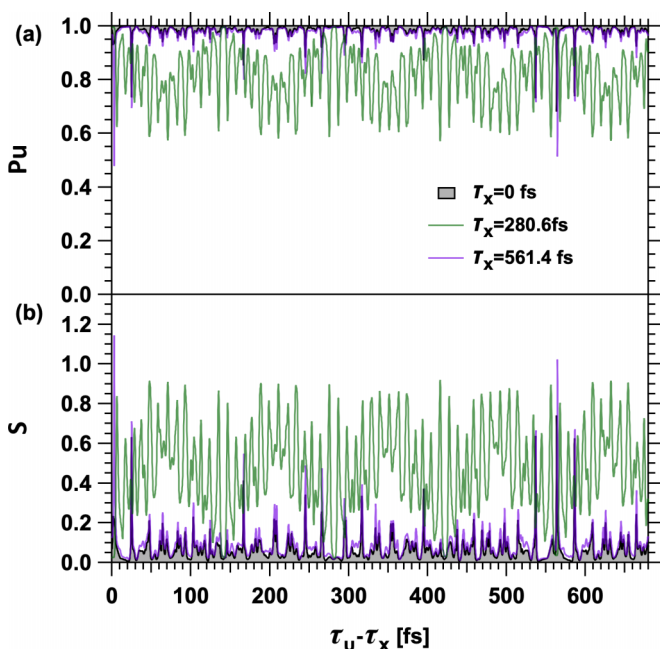


FIG. 8. (a) Evolution of the purity of the reduced density matrix, $\rho_{\text{ion}}^{(2)}(\kappa, \kappa'; \tau_x, \tau_u)$, upon changing the delay of the UV probe pulse. (b) Evolution of the von Neumann entropy of $\rho_{\text{ion}}^{(2)}(\kappa, \kappa'; \tau_x, \tau_u)$. The origin of the delay axis is adjusted to the time delay of the second XUV pulse, τ_x . The reduced density matrices after the photoionization, $\rho_{\text{ion},v''}^{(1)}(\tau_x)$, with τ_x of 0 fs (black solid curve with shaded areas), 280.6 fs (green solid curve), and 561.4 fs (violet solid curve) are adopted, respectively, to calculate the reduced density matrix, $\rho_{\text{ion}}^{(2)}(\kappa, \kappa'; \tau_x, \tau_u)$, given by Eq. (43). The von Neumann entropy of $\rho_{\text{ion},v''}^{(1)}(\tau_x)$ exhibits a local maximum and minimum at times $\tau_x = 280.6$ and 561.4 fs, respectively, shown as arrowed tags in Fig. 2(b).

In the case of $\tau_x = 280.6$ fs, the vibrational wave packet created upon the irradiation of the first XUV pulse is revived and localized around the outer turning point, and the von Neumann entropy of $\rho_{\text{ion},v''}^{(1)}(\tau_x)$ exhibits a local maximum upon the irradiation of the second XUV pulse at this time, as indicated with an arrowed tag in Fig. 2(b). The evolutions of the purity and von Neumann entropy of $\rho_{\text{ion}}^{(2)}(\kappa, \kappa'; \tau_x, \tau_u)$ with $\tau_x = 280.6$ fs are depicted as solid green curves in Figs. 8(a) and 8(b), respectively. Modulations with a period of ≈ 11 fs clearly appear in both curves, and the modulation amplitudes are significantly larger than those emerging in the black and violet curves. We cannot specify the concrete reason for these characteristics of the green curves at present, even though the vibrational motion of the synthesized wave packet might be one of the origins. We show the magnitudes of the reduced density matrices with $\tau_x = 0$ fs and $\tau_x = 280.6$ fs in Figs. 9(a)–9(d) to find the alterations of visible features when the von Neumann entropy S (the purity Pu) changes from one of the local minima (local maxima) to one of the local maxima (local minima) during the scanning of τ_u . By setting τ_x to zero, the XUV pulse pair is reduced to a single XUV pulse. Under this ionization condition, the von Neumann entropy falls into the first local minimum at $\tau_u = 21$ fs as shown in Fig. 8(b). The reduced density matrix uniformly spreads over the region of the off-diagonal elements, as shown in Fig. 9(a), and thus it is reasonable for this reduced density

matrix to show high coherence, demonstrated by a low S of 4.67×10^{-3} and a high Pu of 0.999. The reduced density matrix changes to a structure with the appearance of a four-leaf clover, in which the upper right leaf is enhanced, when the von Neumann entropy reaches the next local maximum by adjusting τ_u to 24.6 fs, as shown in Fig. 9(b). The increase of S to 0.630 and the reduction of Pu to 0.734 might be caused by a moderate concentration of the reduced density matrix in the region around the diagonal elements, whereas these values of S and Pu are far from the extremes of 1.87 and 0.385 obtained from the reduced density matrix shown in Fig. 7, which clearly reveals the features of entanglement. As a result, we expect that the $\text{H} + \text{H}^+$ system is partially entangled with a continuum electron at this moment.

It is worth investigating the visible feature of the reduced density matrix $\rho_{\text{ion}}^{(2)}(\kappa, \kappa'; \tau_x, \tau_u)$ under the condition that the coherence of the reduced density matrix $\rho_{\text{ion},v''}^{(1)}(\tau_x)$ is maximally lost by setting $\tau_x = 280.6$ fs, because $\rho_{\text{ion}}^{(2)}(\kappa, \kappa'; \tau_x, \tau_u)$ regains coherence with S of 2.57×10^{-2} and Pu of 0.995 when $\tau_u = 421.8$ fs ($\tau_u - \tau_x = 141.4$ fs). In fact, we observe a homogeneous distribution of the magnitude of $\rho_{\text{ion}}^{(2)}(\kappa, \kappa'; \tau_x, \tau_u)$ in Fig. 9(c), which might be one of the typical forms of the pure density matrix, as already exhibited in Fig. 9(a). This feature is transformed to the peculiar structure resembling a flying fenghuang, which directs its enriched tail to the bottom-left corner, when 328.2 fs is substituted into τ_u ($\tau_u - \tau_x = 47.8$ fs), as shown in Fig. 9(d). The enriched tail, slightly enhanced body, and weak head are aligned on the diagonal line, while the wings with flight feathers are embedded in the off-diagonal regions. We suppose that the parts on the diagonal line promote the mixture of the reduced density matrix, resulting in $S = 0.911$ and $\text{Pu} = 0.590$.

The analysis of the reduced density matrices after the irradiation of the UV pulse mentioned above is somewhat abstract, and it is not apparent how to evaluate S or Pu from the measured quantities in the experiment. Nevertheless, the analytical form of the reduced density matrix given by Eq. (43) is beneficial for understanding how the coherence among the multiple optical pulses is involved in the composite system of a continuum electron and an $\text{H} + \text{H}^+$ system.

IV. SUMMARY AND PROSPECTS

We have formulated the time-dependent perturbative solutions of the TDSE involving the states in the neutral molecule M system and those in the $e^- \otimes M^+$ system interacting with the coherent optical pulse sequence via dipoles. By adapting the solutions to the H_2 and $e^- \otimes \text{H}_2^+$ systems and imposing the resonant excitation condition, we have successfully obtained analytical formulas describing the state vectors and density matrices that can reproduce the JES and DJKS spectrograms calculated by numerical integration of the TDSE in the preceding studies. Owing to the low computational cost of using the resultant analytical formulas, we have found that the JES can be acquired without resolving the KER of the $\text{H} + \text{H}^+$ system in the actual experiment because the structure of the modulation on the DJKS spectrogram is not significantly changed by accumulating many DJKS spectrograms with different KERs in the calculation. We have explained,

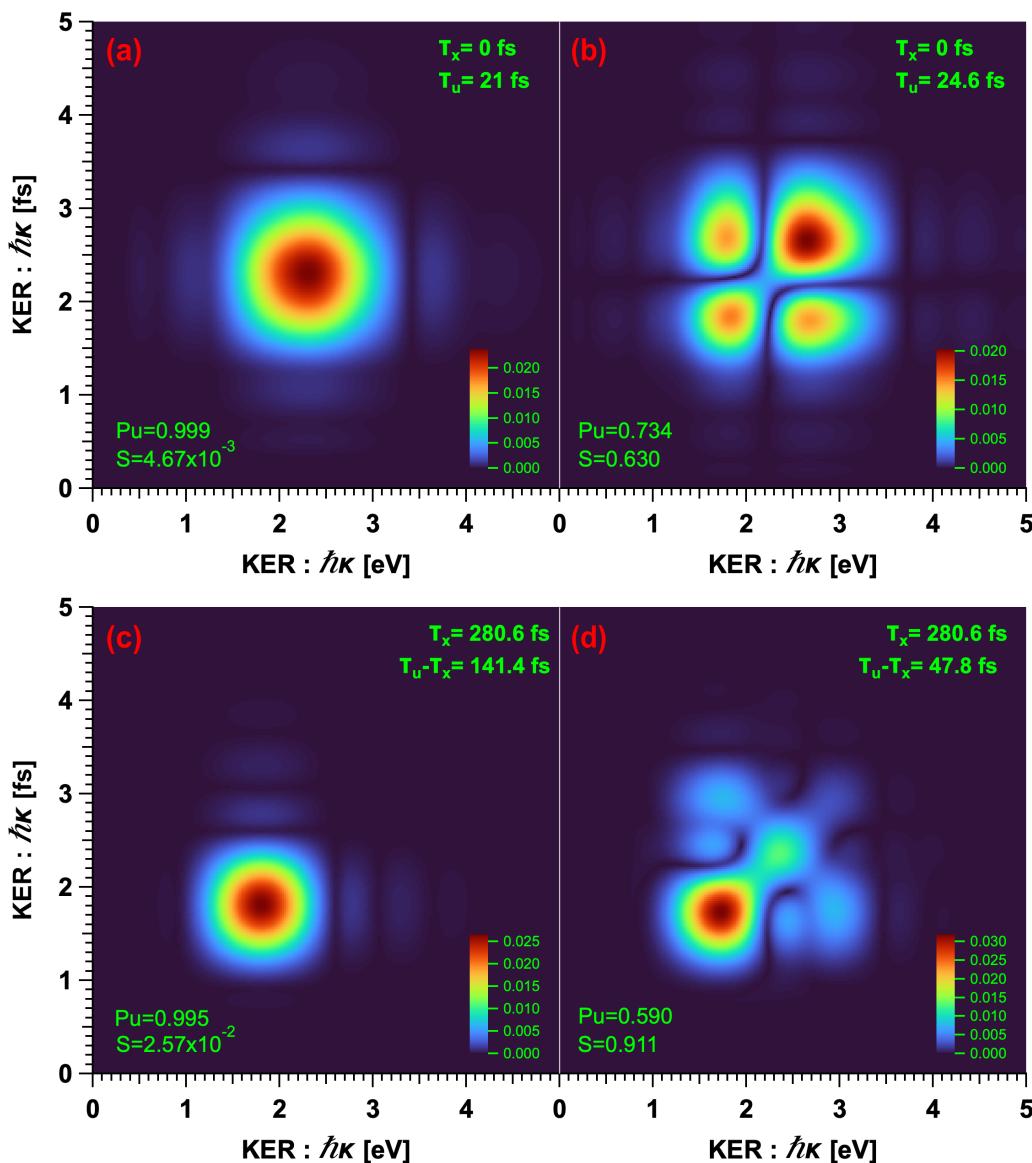


FIG. 9. Magnitudes of reduced density matrices $|\rho_{\text{ion}}^{(2)}(\kappa, \kappa'; \tau_x, \tau_u)|$ at specific values of τ_x and τ_u . (a) $\tau_x = 0$ fs and $\tau_u = 21$ fs set to locally minimize the von Neumann entropy S . (b) $\tau_x = 0$ fs and $\tau_u = 24.6$ fs set to locally maximize S . (c) $\tau_x = 280.6$ fs and $\tau_u = 421.8$ fs set to locally minimize S . (d) $\tau_x = 280.6$ fs and $\tau_u = 328.2$ fs set to locally maximize S . The purity Pu and S are indicated at the bottom-left corner of each figure.

by using the approximated formula of the DJKS spectrogram, that the characteristic of the interference fringes on the DJKS spectrogram originates from the alteration of the modulation amplitude in accordance with the delay between the XUV pulse pair. We also clarify how the off-diagonal elements of the reduced density matrix, which describes the H_2^+ generated immediately after the irradiation of the XUV pulse, disappear upon increasing the GDD of the XUV pulse. We have analyzed the reduced density matrix describing the $H + H^+$ system after the irradiation of the UV pulse by calculating the purity and von Neumann entropy.

One of the most crucial issues in performing the experiment to measure the JES and DJKS spectrogram is the development of a light source that can deliver a coherent XUV pulse pair and a UV pulse with finely adjustable delays among

the three pulses. To this end, we have already developed a hybrid interferometer utilizing the HH pulse of a Ti:sapphire laser pulse [24] as an input. In the hybrid interferometer, the XUV HH pulse is spatially split into two replicas upon reflection near the boundaries of two parallel and closely configured silicon beam splitter mirrors (SiBSs), whereas the UV third harmonic (TH) pulse is also spatially separated from the XUV HH pulse using a dichroic mirror set in front of the SiBSs. The TH pulse is recombined with the XUV pulse pair behind the SiBSs after passing through a delay line configured similarly to a Mach-Zehnder-type interferometer. We confirmed the feasibility of the hybrid interferometer for demonstrating the coherence between the two XUV HH pulses and that between the electronic states excited with the two XUV HH pulses by observing Ramsey-type interference fringes with a

period of 200 as emerging from the $2p$ excited state in a He atom [25].

Another important issue is how to measure the JES of a continuum electron and $H + H^+$ system. We assume that the coincidence measurement scheme of an electron and an ion performed with existing technologies is suitable and sufficient for measuring the JES. The magnetic-bottle multi-electron-ion coincidence spectrometer developed by Matsuda *et al.* is one of the most appropriate devices for such measurement [26]. This device is basically composed of a time-of-flight (TOF) electron spectrometer with a static magnetic field to guide photoelectrons to a microchannel plate (MCP). The remaining ions left behind the photoelectrons are accelerated with electrodes, to which pulsed high voltages are applied after the arrival of the photoelectrons at the MCP. A detection event of one electron can be utilized as a trigger of the pulsed high voltage to the electrodes by reducing the target gas density, so as to decrease the rate of electron detection to less than one per laser shot. As a result, the ion that emits the detected photoelectron can also be recorded in the same TOF spectrum. This device played a crucial role in identifying that the $4d^{-2}$ double core-hole state of a Xe atom generated by the two-photon absorption of 91-eV photons made a major contribution to the Xe^{4+} yield [27] and in resolving the transient core-hole resonances in Kr [28].

We are now considering how to perform the actual experiment by utilizing our interferometer and other devices, and we hope to obtain an experimental demonstration of our theoretical model in the future.

ACKNOWLEDGMENTS

We acknowledge financial support from Core Research for Evolutionary Science and Technology (CREST) (Grant No. JPMJCR15N1), from the Japan Science and Technology Agency, Japan; Grants-in-Aid for Scientific Research (Grants No. 26247068, No. 26220606, and No. 22K18324) from the Ministry of Education, Culture, Sports, Science and Technology (MEXT), Japan; and the Quantum Leap Flagship Program (Grant No. JPMXS0118068681) from MEXT.

APPENDIX A: TIME-DEPENDENT PERTURBATION THEORY

1. Basis set

a. Neutral molecule

It is useful to adopt the eigenstates of the molecular Hamiltonian as the basis set to expand the general states of a molecular system in time-dependent perturbation theory. When a molecule contains N electrons and M nuclei, the Hamiltonian of this molecular system may be described as

$$H(\mathbf{R}, \mathbf{r}) = - \sum_{n=1}^N \frac{\hbar^2}{2m_e} \frac{\partial^2}{\partial \mathbf{r}_n^2} - \sum_{m=1}^M \frac{\hbar^2}{2M_m} \frac{\partial^2}{\partial \mathbf{R}_m^2} + V(\mathbf{R}, \mathbf{r}), \quad (\text{A1})$$

where the electron and nuclear coordinates are defined as $\mathbf{r} = (\mathbf{r}_1, \mathbf{r}_2, \dots, \mathbf{r}_N)$ and $\mathbf{R} = (\mathbf{R}_1, \mathbf{R}_2, \dots, \mathbf{R}_M)$, respectively. We specify the mass of the m th nucleus as M_m and that of an electron as m_e . The potential term $V(\mathbf{R}, \mathbf{r})$ is composed of

the linear summation of the Coulomb potentials describing the interaction between electrons, that between nuclei, and that between electrons and nuclei. In accordance with the conventional method [29], we assume that the wave function $\Psi(\mathbf{R}, \mathbf{r})$ satisfies the eigenequation

$$H(\mathbf{R}, \mathbf{r})\Psi(\mathbf{R}, \mathbf{r}) = E\Psi(\mathbf{R}, \mathbf{r}) \quad (\text{A2})$$

and that $\Psi(\mathbf{R}, \mathbf{r})$ can be expressed as a product of the wave function of the electronic system ${}_N\langle \mathbf{r} | \psi_{e_\alpha}(\mathbf{R}) \rangle = \psi_{e_\alpha}(\mathbf{R}, \mathbf{r})$ specified by electronic quantum number α , which parametrically depends on \mathbf{R} , and the coefficient function $\phi_\alpha(\mathbf{R})$; thus, we write

$$\Psi(\mathbf{R}, \mathbf{r}) = \Psi_\alpha(\mathbf{R}, \mathbf{r}) = \phi_\alpha(\mathbf{R})\psi_{e_\alpha}(\mathbf{R}, \mathbf{r}), \quad (\text{A3})$$

where E in Eq. (A2) is the total eigenenergy of the molecule as a composite system of electrons and nuclei. The electronic wave function $\psi_{e_\alpha}(\mathbf{R}, \mathbf{r})$ should satisfy the following eigenequation for the electronic system:

$$-\sum_{n=1}^N \frac{\hbar^2}{2m_e} \frac{\partial^2 \psi_{e_\alpha}(\mathbf{R}, \mathbf{r})}{\partial \mathbf{r}_n^2} + V(\mathbf{R}, \mathbf{r})\psi_{e_\alpha}(\mathbf{R}, \mathbf{r}) = V_{e_\alpha}(\mathbf{R})\psi_{e_\alpha}(\mathbf{R}, \mathbf{r}). \quad (\text{A4})$$

The eigenenergy of electronic state α , $V_{e_\alpha}(\mathbf{R})$, parametrically changes with respect to \mathbf{R} . We assume that the state set $|\psi_{e_\alpha}(\mathbf{R})\rangle$ is orthonormal to satisfy $\langle \psi_{e_\alpha}(\mathbf{R}) | \psi_{e_\beta}(\mathbf{R}) \rangle = \int d^{3N} \mathbf{r} \psi_{e_\alpha}^*(\mathbf{R}, \mathbf{r}) \psi_{e_\beta}(\mathbf{R}, \mathbf{r}) = \delta_{\alpha\beta}$.

By substituting Eq. (A3) into Eq. (A2) and performing the adiabatic approximation [neglecting cross terms involving different electronic states such as $\int d^{3N} \mathbf{r} \psi_{e_\alpha}^*(\mathbf{R}, \mathbf{r}) \frac{\partial \psi_{e_\beta}(\mathbf{R}, \mathbf{r})}{\partial \mathbf{R}}$] and the BO approximation [neglecting $\int d^{3N} \mathbf{r} \psi_{e_\alpha}^*(\mathbf{R}, \mathbf{r}) T_{nc}(\mathbf{R}) \psi_{e_\alpha}(\mathbf{R}, \mathbf{r})$] [29], the coefficient $\phi_\alpha(\mathbf{R})$ should also satisfy the eigenequation

$$-\sum_{m=1}^M \frac{\hbar^2}{2M_m} \frac{\partial^2 \phi_\alpha(\mathbf{R})}{\partial \mathbf{R}_m^2} + V_{e_\alpha}(\mathbf{R})\phi_\alpha(\mathbf{R}) = E\phi_\alpha(\mathbf{R}), \quad (\text{A5})$$

and, thus, $\phi_\alpha(\mathbf{R})$ should be regarded as a wave function of the nuclei in the adiabatic potential $V_{e_\alpha}(\mathbf{R})$.

Actually, the nuclear wave function should be classified by quantum numbers depending on the degrees of the nuclear motion; thus, we add a quantum number v to $\phi_\alpha(\mathbf{R})$ and E as a superscript and add α as a subscript to E to identify the nuclear and electronic states, namely, $\phi_\alpha(\mathbf{R}) \rightarrow \phi_\alpha^v(\mathbf{R})$ and $E \rightarrow E_\alpha^v$ in Eq. (A5) and $\phi_\alpha(\mathbf{R})\psi_{e_\alpha}(\mathbf{R}, \mathbf{r}) \rightarrow \phi_\alpha^v(\mathbf{R})\psi_{e_\alpha}(\mathbf{R}, \mathbf{r})$ in Eq. (A3). The quantum number v may be discrete or continuous depending on the state of the nuclei. Note that the eigenenergy $E = E_\alpha^v$ in Eq. (A5), whose solutions express the states of the nuclei, coincides with the total energy of the composite system. As a result, Eq. (A2) is rewritten as

$$H(\mathbf{R}, \mathbf{r})\Psi_\alpha^v(\mathbf{R}, \mathbf{r}) = E_\alpha^v\Psi_\alpha^v(\mathbf{R}, \mathbf{r}). \quad (\text{A6})$$

By imposing the orthonormal property on the nuclear wave-function set, which is expressed as $\int d^{3M} \mathbf{R} \phi_\alpha^{v*}(\mathbf{R}) \phi_\alpha^{v'}(\mathbf{R}) = \delta_{vv'}$ or $\delta(v - v')$, the total wave-function set of the composite system, $\Psi_\alpha^v(\mathbf{R}, \mathbf{r}) = \phi_\alpha^v(\mathbf{R})\psi_{e_\alpha}(\mathbf{R}, \mathbf{r})$ [or the state vector set

$|\Psi_\alpha^v(\mathbf{R})\rangle = \phi_\alpha^v(\mathbf{R})|\psi_{e_\alpha}(\mathbf{R})\rangle$, is also orthonormal:

$$\begin{aligned} & \int d^{3M} \mathbf{R} \langle \Psi_\alpha^v(\mathbf{R}) | \Psi_\beta^{v'}(\mathbf{R}) \rangle \\ &= \int d^{3M} \mathbf{R} \phi_\alpha^{v*}(\mathbf{R}) \phi_\beta^{v'}(\mathbf{R}) \langle \psi_{e_\alpha}(\mathbf{R}) | \psi_{e_\beta}(\mathbf{R}) \rangle \\ &= \delta_{\alpha\beta} \int d^{3M} \mathbf{R} \phi_\alpha^{v*}(\mathbf{R}) \phi_\alpha^{v'}(\mathbf{R}) = \begin{cases} \delta_{\alpha\beta} \delta_{vv'}, & \text{or} \\ \delta_{\alpha\beta} \delta(v - v'). \end{cases} \end{aligned} \quad (\text{A7})$$

Thus, we define the projection operator on the neutral molecule states as

$$\hat{P}(\mathbf{R}; \mathbf{R}') = \sum_\alpha \sum_v \int d^{3M} \mathbf{R} |\Psi_\alpha^v(\mathbf{R})\rangle \langle \Psi_\alpha^v(\mathbf{R}')|, \quad (\text{A8})$$

and its $(\mathbf{r}, \mathbf{r}')$ element is described as $P(\mathbf{R}, \mathbf{r}; \mathbf{R}', \mathbf{r}') = \sum_\alpha \sum_v \Psi_\alpha^v(\mathbf{R}, \mathbf{r}) \Psi_\alpha^{v*}(\mathbf{R}', \mathbf{r}')$. The characteristic of the projection described as $\int d^{3M} \mathbf{R}' \hat{P}(\mathbf{R}; \mathbf{R}') \hat{P}(\mathbf{R}'; \mathbf{R}'') = \hat{P}(\mathbf{R}; \mathbf{R}'')$ can be confirmed by using the orthonormal property of the state vector in Eq. (A7).

b. Molecular ion + continuum electron

After the ionization of the molecule, the molecular system is composed of a molecular ion containing $N - 1$ electrons and M nuclei, which may be described as a wave function $\Psi^+(\mathbf{R}, \mathbf{r}^+)$ and a continuum electronic wave function $\psi_{c_\alpha}(\omega_e; \mathbf{R}, \mathbf{r})$, where we describe the coordinates of $N - 1$ electrons in the molecular ion as $\mathbf{r}^+ = (\mathbf{r}_1, \mathbf{r}_2, \dots, \mathbf{r}_{N-1})$ and the KE of the continuum electron as $\hbar\omega_e$. Note that we cannot actually specify which electron is detached upon ionization; thus, we must consider all possible electron coordinates and symmetries of the continuum electron when we adopt a more rigorous model. Nevertheless, we have simplified the situation because our aim is only to explore whether the total wave function of a (molecular ion + continuum electron) composite system may approximate the eigenfunction of the total Hamiltonian described in Eq. (A1).

To this end, we divide $H(\mathbf{R}, \mathbf{r})$ into two parts:

$$H(\mathbf{R}, \mathbf{r}) = H^+(\mathbf{R}, \mathbf{r}^+) + H_c(\mathbf{R}, \mathbf{r}) \quad (\text{A9})$$

where we define $H^+(\mathbf{R}, \mathbf{r}^+)$ as

$$\begin{aligned} H^+(\mathbf{R}, \mathbf{r}^+) &\equiv - \sum_{n=1}^{N-1} \frac{\hbar^2}{2m_e} \frac{\partial^2}{\partial \mathbf{r}_n^2} - \sum_{m=1}^M \frac{\hbar^2}{2M_m} \frac{\partial^2}{\partial \mathbf{R}_m^2} + V^+(\mathbf{R}, \mathbf{r}^+), \end{aligned} \quad (\text{A10})$$

and

$$H_c(\mathbf{R}, \mathbf{r}) \equiv - \frac{\hbar^2}{2m_e} \frac{\partial^2}{\partial \mathbf{r}_N^2} + V_c(\mathbf{R}, \mathbf{r}). \quad (\text{A11})$$

The potential denoted as $V^+(\mathbf{R}, \mathbf{r}^+)$ in Eq. (A10) is a part that is independent of the N th electron coordinate \mathbf{r}_N in $V(\mathbf{R}, \mathbf{r})$. The remainder of $V(\mathbf{R}, \mathbf{r})$ is defined as $V_c(\mathbf{R}, \mathbf{r})$ which may be written as $V_c(\mathbf{R}, \mathbf{r}) = \frac{1}{4\pi\epsilon_0} \sum_{n=1}^{N-1} \frac{q_e^2}{|\mathbf{r}_n - \mathbf{r}_N|} - \frac{1}{4\pi\epsilon_0} \sum_{m=1}^M \frac{Z_m q_e^2}{|\mathbf{R}_m - \mathbf{r}_N|}$. The dielectric constant of vacuum, the charge of an electron, and the charge number of the m th nucleus are denoted as ϵ_0 , q_e , and Z_m , respectively. Because we consider a continuum electron situated far from the molecular ion, we approximate

$V_c(\mathbf{R}, \mathbf{r})$ as the effective potential $V_c(\mathbf{r}_N)$:

$$V_c(\mathbf{R}, \mathbf{r}) \sim V_c(\mathbf{r}_N) = - \frac{1}{4\pi\epsilon_0} \frac{q_e^2 f(\mathbf{r}_N)}{|\mathbf{r}_N|}. \quad (\text{A12})$$

The function $f(\mathbf{r}_N)$ should be adjusted to mimic $V_c(\mathbf{R}, \mathbf{r})$ under the conditions $|\mathbf{r}_N| \gg |\mathbf{r}_n|$ ($N > n$) and $|\mathbf{r}_N| \gg |\mathbf{R}_m|$. With this approximation, the Hamiltonian $H_c(\mathbf{R}, \mathbf{r})$ is simplified to $H_c(\mathbf{r}_N) = -\frac{\hbar^2}{2m_e} \frac{\partial^2}{\partial \mathbf{r}_N^2} + V_c(\mathbf{r}_N)$, expressing a one-electron system; thus, we assume the continuum electron function $\psi_{c_\alpha}(\omega_e; \mathbf{r}_N)$ to be independent of \mathbf{R} and \mathbf{r}^+ , and the continuum electron function satisfies the following eigenequation:

$$H_c(\mathbf{r}_N) \psi_{c_\alpha}(\omega_e; \mathbf{r}_N) = \hbar\omega_e \psi_{c_\alpha}(\omega_e; \mathbf{r}_N). \quad (\text{A13})$$

We substitute quantum number α in the wave function in Eq. (A13) to express the correlation with the electronic state in the molecular ion identified by α . We also impose the orthonormal property on $\psi_{c_\alpha}(\omega_e; \mathbf{r}_N)$.

The molecular ion left behind the continuum electron is governed by the Hamiltonian $H^+(\mathbf{R}, \mathbf{r}^+)$ in Eq. (A10), the form of which is equivalent to that of $H(\mathbf{R}, \mathbf{r})$ in Eq. (A1) except that the number of electrons is reduced to $N - 1$. Therefore, we constitute the wave function of the molecular ion $\Psi_\alpha^{+v'}(\mathbf{R}, \mathbf{r}^+)$ as a product of the nuclear wave function $\phi_\alpha^{+v'}(\mathbf{R})$ and the electronic wave function $\psi_{e_\alpha}^+(\mathbf{R}, \mathbf{r}^+)$, $\Psi_\alpha^{+v'}(\mathbf{R}, \mathbf{r}^+) = \phi_\alpha^{+v'}(\mathbf{R}) \psi_{e_\alpha}^+(\mathbf{R}, \mathbf{r}^+)$, under the adiabatic and BO approximations. The wave function of the molecular ion satisfies an eigenequation similar to Eq. (A6) for the neutral molecule as follows:

$$H^+(\mathbf{R}, \mathbf{r}^+) \Psi_\alpha^{+v'}(\mathbf{R}, \mathbf{r}^+) \simeq E_\alpha^{+v'} \Psi_\alpha^{+v'}(\mathbf{R}, \mathbf{r}^+), \quad (\text{A14})$$

where $E_\alpha^{+v'}$ is the total energy of the molecular ion of the v' th vibrational state in the α -electric state. We impose the normalization and completeness conditions similar to Eqs. (A7) and (A8) on the wave function $\Psi_\alpha^{+v'}(\mathbf{R}, \mathbf{r}^+)$.

Under these approximated conditions, the product of the wave function of the molecular ion $\Psi_\alpha^{+v'}(\mathbf{R}, \mathbf{r}^+)$ and the wave function of the continuum electron $\psi_{c_\alpha}(\omega_e; \mathbf{r}_N)$ can be an approximated eigenfunction of $H(\mathbf{R}, \mathbf{r})$ satisfying

$$\begin{aligned} & H(\mathbf{R}, \mathbf{r}) \Psi_\alpha^{+v'}(\mathbf{R}, \mathbf{r}^+) \psi_{c_\alpha}(\omega_e; \mathbf{r}_N) \\ & \simeq (E_\alpha^{+v'} + \hbar\omega_e) \Psi_\alpha^{+v'}(\mathbf{R}, \mathbf{r}^+) \psi_{c_\alpha}(\omega_e; \mathbf{r}_N), \end{aligned} \quad (\text{A15})$$

because we have neglected the \mathbf{R} dependence and \mathbf{r}^+ dependence in the wave function of the continuum electron $\psi_{c_\alpha}(\omega_e; \mathbf{r}_N)$. Thus, we treat the wave function of $\Phi_\alpha^{+v'}(\omega_e; \mathbf{R}, \mathbf{r}) \equiv \Psi_\alpha^{+v'}(\mathbf{R}, \mathbf{r}^+) \psi_{c_\alpha}(\omega_e; \mathbf{r}_N)$ as an eigenfunction of the total Hamiltonian $H(\mathbf{R}, \mathbf{r})$ and impose orthonormality:

$$\begin{aligned} & \int d^{3M} \mathbf{R} \langle \Phi_\alpha^{+v'}(\omega_e'; \mathbf{R}) | \Phi_\beta^{+v''}(\omega_e''; \mathbf{R}) \rangle \\ &= \begin{cases} \delta_{\alpha\beta} \delta_{v'v''} \delta(\omega_e' - \omega_e''), & \text{or} \\ \delta_{\alpha\beta} \delta(v' - v'') \delta(\omega_e' - \omega_e''). \end{cases} \end{aligned} \quad (\text{A16})$$

Then, the projection operator $\hat{P}^+(\mathbf{R}; \mathbf{R}')$ to the states involving a molecular ion and a continuum electron is described as

$$\hat{P}^+(\mathbf{R}; \mathbf{R}') = \sum_{\alpha} \sum_{\nu'} \int_0^{\infty} d\omega_e |\Phi_{\alpha}^{+\nu'}(\omega_e; \mathbf{R})\rangle \langle \Phi_{\alpha}^{+\nu'}(\omega_e; \mathbf{R}')|, \quad (\text{A17})$$

which is similar to Eq. (A8).

2. Perturbative solution of the TDSE

We assume that the TDSE of our model has the following conventional form:

$$i\hbar \frac{\partial}{\partial t} |\Psi(\mathbf{R}; t)\rangle = \{\hat{H}(\mathbf{R}) + \hat{V}(t)\} |\Psi(\mathbf{R}; t)\rangle, \quad (\text{A18})$$

where the $(\mathbf{r}, \mathbf{r}')$ component of the molecular Hamiltonian operator $\hat{H}(\mathbf{R})$ is described using $H(\mathbf{R}, \mathbf{r})$ in Eq. (A1) so as to satisfy $\langle \mathbf{r} | \hat{H}(\mathbf{R}) | \mathbf{r}' \rangle = H(\mathbf{R}, \mathbf{r}) \delta^{3N}(\mathbf{r} - \mathbf{r}')$. We adopt the dipole interaction between the linear polarized electric field of the coherent superposition of the incident optical pulses involving a pair of XUV pulses and a UV pulse. Therefore, the interaction Hamiltonian operator $\hat{V}(t)$ can be expressed as $\hat{V}(t) = \hat{\mu}E(t)$, where $\hat{\mu}$ is a dipole operator projected onto

the polarization direction and $E(t)$ is the complex amplitude of the total electric field of the incident optical pulses. We neglect the negative frequency part of the electric field contributing to the photoemission accompanied by deexcitation and recombination processes for simplicity, so that $E(t)$ is a complex number and the magnitude of its FT exhibits peaks only in the region where the frequency is positive. We specify the form of $E(t)$ as

$$\begin{aligned} E(t) &= E_x(t) + E_x(t - \tau_x) + E_u(t - \tau_u) \\ &= E_x(t; \tau_x) + E_u(t - \tau_u), \end{aligned} \quad (\text{A19})$$

where $E_x(t)$ is the electric field of an XUV pulse and $E_x(t - \tau_x)$ is its replica with delay τ_x . The electric field of the UV pulse with delay τ_u is expressed as $E_u(t - \tau_u)$. We also define $E_x(t; \tau_x) \equiv E_x(t) + E_x(t - \tau_x)$ to simplify the following equations.

According to the convention of the time-dependent perturbation theory, we change the form of the TDSE using the state vector in the interaction picture, implement successive integration and substitution, and finally reconvert the state vector into the Schrödinger picture. The resultant solution is

$$\begin{aligned} |\Psi(\mathbf{R}; t)\rangle &= e^{\frac{i\hat{H}(\mathbf{R})}{\hbar}(t-t_0)} |\Psi(\mathbf{R}; t_0)\rangle + \frac{1}{i\hbar} \int_{t_0}^t dt_1 e^{\frac{i\hat{H}(\mathbf{R})}{\hbar}(t-t_1)} \hat{V}(t_1) e^{\frac{i\hat{H}(\mathbf{R})}{\hbar}(t_1-t_0)} |\Psi(\mathbf{R}; t_0)\rangle \\ &+ \left(\frac{1}{i\hbar}\right)^2 \int_{t_0}^t dt_1 \int_{t_0}^{t_1} dt_2 e^{\frac{i\hat{H}(\mathbf{R})}{\hbar}(t-t_1)} \hat{V}(t_1) e^{\frac{i\hat{H}(\mathbf{R})}{\hbar}(t_1-t_2)} \hat{V}(t_2) e^{\frac{i\hat{H}(\mathbf{R})}{\hbar}(t_2-t_0)} |\Psi(\mathbf{R}; t_0)\rangle + \dots, \end{aligned} \quad (\text{A20})$$

where $|\Psi(\mathbf{R}; t_0)\rangle$ is the initial state vector at the initial time t_0 . We focus on analyzing the second and third terms on the right-hand side of Eq. (A20), which involve the one-photon and two-photon interactions, respectively.

APPENDIX B: SPECIFIC FORMS OF TIME-ORDERED INTEGRATION AMPLITUDE

1. Square Lorentz function

We evaluate the time-ordered integration amplitude, $S_{ux}(\Omega_1, \Omega_2; \tau_x, \tau_u)$, given by Eq. (30) or Eq. (31) by assuming specific forms of the envelope function of the XUV and UV pulses. First, we apply the square of the Lorentz function to both $\tilde{A}_u(\Omega)$ and $\tilde{A}_x(\Omega)$ with the same bandwidth of $\delta\Omega$, namely,

$$\tilde{A}_{u,x}(\Omega) = \tilde{A}_{0,u,x} \left(\frac{\Omega^2}{\delta\Omega^2} + 1 \right)^{-2}, \quad (\text{B1})$$

where we neglect the chirp in both pulses, and thus Fourier limit pulses are assumed. The temporal profiles of the envelope functions, $A_{u,x}(t) = \frac{1}{2\pi} \int d\Omega \tilde{A}_{u,x}(\Omega) e^{-i\Omega t}$, are given by

$$A_{u,x}(t) = \frac{\delta\Omega \tilde{A}_{0,u,x}}{4} (\delta\Omega|t| + 1) e^{-\delta\Omega|t|}. \quad (\text{B2})$$

The left-side and right-side time derivatives at $t = 0$ of the time envelope function in Eq. (B2) are both zero and the envelope function smoothly changes at $t = 0$. This property is sig-

nificantly different from the discontinuous time derivatives of the double-sided exponential function obtained by the inverse FT of the conventional Lorentz function. Because the Fourier transform of the XUV pulse pair is described as the linear summation of $\tilde{A}_x(\Omega - \omega_x)$ and $\tilde{A}_x(\Omega - \omega_x) e^{i\Omega\tau_x}$, [$\tilde{E}_x(\Omega; \tau_x) = \tilde{E}_x(\Omega)(1 + e^{i\Omega\tau_x}) = \tilde{A}_x(\Omega - \omega_x)(1 + e^{i\Omega\tau_x})$], we only evaluate the contribution from the first XUV pulse, and we calculate the time-ordered integration amplitude $S_{ux}(\Omega_1, \Omega_2; \tau_u)$, which is obtained by replacing $\tilde{A}_x(\Omega_2 - \omega_x)$ with $\tilde{A}_x(\Omega_2 - \omega_x)$ on the right-hand side of Eq. (31). The contribution from the τ_x -delayed XUV pulse is obtained by replacing τ_u with $\tau_u - \tau_x$ in $S_{ux}(\Omega_1, \Omega_2; \tau_u)$ and multiplying by the phase factor $e^{i\Omega_2\tau_x}$.

Before evaluating $S_{ux}(\Omega_1, \Omega_2; \tau_u)$, we symmetrize the parameters contained in the arguments of \tilde{A}_u and \tilde{A}_x so as to clearly show the spectral peak difference of \tilde{A}_u and \tilde{A}_x and the detuning from the resonance. The following two parameters are introduced:

$$\begin{aligned} \omega &\equiv \Omega_1 + \Omega_2 - \omega_u - \omega_x \\ &= \omega'_e - \{\omega_u + \omega_x - (\kappa' + \kappa_0 - \omega_g^0)\}, \quad (\text{B3}) \\ \Delta &\equiv \{(\Omega_1 - \omega_u) - (\Omega_2 - \omega_x)\}/2 \\ &= \{\kappa' + \kappa_0 - \omega^{+\nu'} - \omega_u\} \\ &\quad - \{\omega'_e + \omega^{+\nu'} - \omega_g^0 - \omega_x\}/2. \end{aligned} \quad (\text{B4})$$

These parameters are graphically indicated in Fig. 10(a). The parameter ω expresses the difference between the peak an-

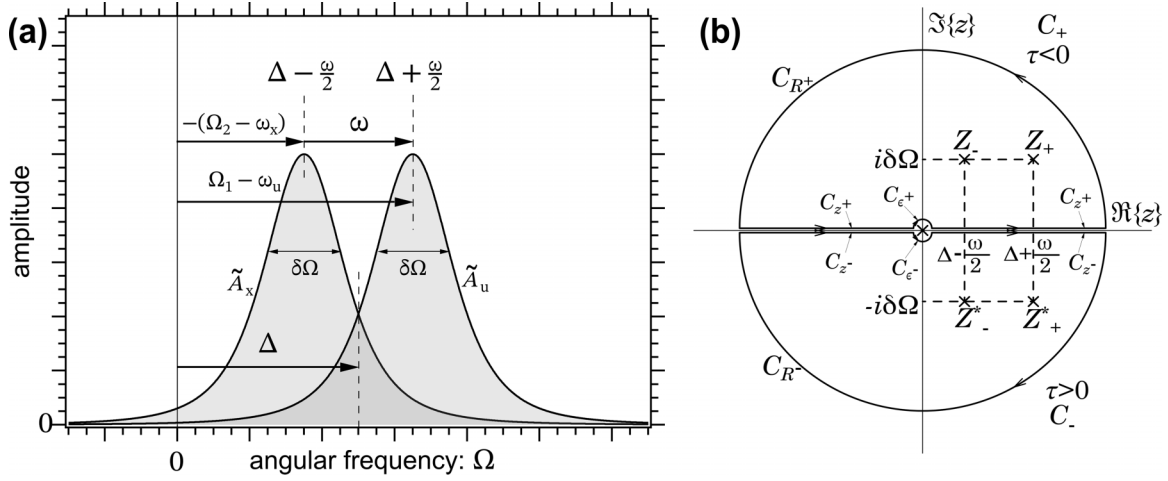


FIG. 10. (a) Schematic of the spectral amplitudes of an XUV pulse and a UV pulse. (b) Poles and contours relevant for calculating the PVI of Eq. (B10). Poles of the integrand $f_{\text{SL}}(z)$ in Eq. (B11) are depicted as crossings. The closed semicircle contour adopted for calculating the PVI of Eq. (B10) for $\tau_u > 0$ in the lower half plane is labeled C_- , which is composed of the two lines on the real axis excluding the origin, named C_{z^-} , the open semicircle around the origin with an infinitesimal radius, named C_{ϵ^-} , and the open semicircle with a radius of R , named C_{R^-} . The closed semicircle contour for $\tau_u < 0$ is also depicted in the upper half plane with a label of C_+ .

angular frequency of the spectral amplitude of the UV pulse and that of the XUV pulse. The parameter Δ is the central frequency of the product of the two spectral amplitudes $\tilde{A}_u(\Omega_1 - \omega_u - \Omega)\tilde{A}_x(\Omega_2 - \omega_x + \Omega)$. The resonance condition is satisfied by adjusting Δ to zero. Note that ω should be sufficiently small in order that the product of the two spectral amplitudes makes a significant contribution to the PVI owing to the sufficient spectral overlap. Therefore, the PVI should be finite only in the region around $\omega \approx 0 \Leftrightarrow \omega'_e \sim \omega_u + \omega_x - (\kappa' + \kappa_0 - \omega_g^0)$ from Eq. (B3), which is equivalent to the condition that the KE of the continuum electron $\hbar\omega'_e$ must be approximately equal to the excess energy of two photons after the excitation from the ground vibrational state in the $X^1\Sigma_g^+$ state in H_2 with energy $\hbar\omega_g^0$ to the $2p\sigma_u$ state with energy $\hbar(\kappa' + \kappa_0)$ in H_2^+ , resulting in the description of the energy conservation. Substituting this approximated equation to Eq. (B4), we find that the approximated equation of $\Delta \sim (\kappa' + \kappa_0 - \omega^{+v'}) - \omega_u$ should hold. The terms in the parentheses on the right-hand side of this approximated equation express the excitation energy from the v' th vibrational state in the $1s\sigma_g$ state to the $2p\sigma_u$ state with energy $\kappa' + \kappa_0$ in H_2^+ ; thus, $-\Delta$ can be regarded as the detuning of the photon energy of the UV pulse from the excitation energy. This is the reason why we identify the condition of $\Delta = 0$ to be the condition of resonance.

Using ω and Δ , the time-ordered integration amplitude $S_{\text{ux}}(\Omega_1, \Omega_2; \tau_u)$ is transformed to

$$\begin{aligned} & S_{\text{ux}}\left(\Delta + \frac{\omega}{2} + \omega_u, -\Delta + \frac{\omega}{2} + \omega_x; \tau_u\right) e^{-i(\Delta + \frac{\omega}{2} + \omega_u)\tau_u} \\ &= -\frac{1}{2i\pi} T(\Delta, \omega; \tau_u) + \frac{1}{2} \tilde{A}_u\left(\Delta + \frac{\omega}{2}\right) \tilde{A}_x\left(-\Delta + \frac{\omega}{2}\right), \end{aligned} \quad (\text{B5})$$

where we define the PVI as

$$\begin{aligned} & T(\Delta, \omega; \tau_u) \\ & \equiv \mathcal{P} \int d\Omega \frac{\tilde{A}_u(\Delta + \frac{\omega}{2} - \Omega) \tilde{A}_x[\Omega - (\Delta - \frac{\omega}{2})] e^{-i\Omega\tau_u}}{\Omega} \end{aligned} \quad (\text{B6})$$

$$= \mathcal{P} \int d\Omega \frac{\tilde{A}_u(\omega - \Omega) \tilde{A}_x(\Omega) e^{-i\Omega\tau_u}}{\Omega + (\Delta - \frac{\omega}{2})} e^{-i(\Delta - \frac{\omega}{2})\tau_u}. \quad (\text{B7})$$

Before we perform the integration in Eq. (B6) by substituting the square Lorentz function defined in Eq. (B1) into $\tilde{A}_u(\Omega)$ and $\tilde{A}_x(\Omega)$ as one of the candidate-specific forms, we present the asymptotic form of the amplitudes $T(\Delta, \omega; \tau_u)$ and $S_{\text{ux}}(\Delta + \frac{\omega}{2} + \omega_u, -\Delta + \frac{\omega}{2} + \omega_x; \tau_u)$ by utilizing Eq. (B7) without assuming the specific forms of $\tilde{A}_u(\Omega)$ and $\tilde{A}_x(\Omega)$ when the detuning is sufficiently large for the off-resonance condition $|\Delta| \gg \delta\Omega$ to be satisfied. We can neglect the contribution near the pole at $\Omega = -\Delta + \frac{\omega}{2}$ in the PVI because the magnitude of the numerator $\tilde{A}_u(\Delta + \frac{\omega}{2}) \tilde{A}_x(-\Delta + \frac{\omega}{2})$ is negligibly small due to the off-resonance condition. Thus, the amplitude $T(\Delta, \omega; \tau_u)$ can be approximately equal to $\Delta^{-1} \int d\Omega \tilde{A}_u(\omega - \Omega) \tilde{A}_x(\Omega) e^{-i\Omega\tau_u} e^{-i(\Delta - \frac{\omega}{2})\tau_u}$, and the asymptotic form of the amplitude $S_{\text{ux}}(\Delta + \frac{\omega}{2} + \omega_u, -\Delta + \frac{\omega}{2} + \omega_x; \tau_u)$ may be written as

$$\begin{aligned} & S_{\text{ux}}\left(\Delta + \frac{\omega}{2} + \omega_u, -\Delta + \frac{\omega}{2} + \omega_x; \tau_u\right) \\ & \simeq -\frac{1}{2i\pi} \frac{T_{\text{FROG}_{\text{ux}}}(\omega; \tau_u)}{\Delta} e^{-i(\omega + \omega_u)\tau_u}, \quad (|\Delta| \gg \delta\Omega), \end{aligned} \quad (\text{B8})$$

where we define the amplitude $T_{\text{FROG}_{\text{ux}}}(\omega; \tau_u)$ as

$$T_{\text{FROG}_{\text{ux}}}(\omega; \tau_u) \equiv \int d\Omega \tilde{A}_u(\omega - \Omega) \tilde{A}_x(\Omega) e^{-i\Omega\tau_u}. \quad (\text{B9})$$

This amplitude $T_{\text{FROG}_{\text{ix}}}(\omega; \tau_u)$ coincides with the frequency-resolved correlation amplitude between the two optical pulses, $\tilde{A}_u(\Omega)$ and $\tilde{A}_x(\Omega)$, and it is utilized to retrieve the characteristics of the optical pulses in the method of frequency-resolved optical gating (FROG) [30,31]. Note that the amplitude $\tilde{A}_u(\Omega)$ may be replaced by $\tilde{A}_x(\Omega)$ when we would like to express the autocorrelation FROG of the XUV pulse. The correlation trace between the two pulses is obtained by calculating $\int d\omega |T_{\text{FROG}_{\text{ix}}}(\omega; \tau_u)|^2$, which is proportional to the ion yield from a specific pathway of two-photon ionization. This is the reason why we obtained the autocorrelation traces of the XUV APT by observing the fragment ion yields from simple molecules upon changing the delay between the two replicas of the APT in our past experiments [19,32]. In fact, the asymptotic form of the double time integration amplitude in Eq. (B8) is common for any electronic state whose quantum numbers are summed on the right-hand side of Eq. (26) but whose parameters Δ and ω are different in each electronic state. Therefore, the autocorrelation trace should be distorted with the molecular response function originating from Eqs. (25) and (26), as we pointed out in Ref. [33] and the supplemental document of Ref. [19].

We explore the exact form of $T(\Delta, \omega; \tau_u)$ by adapting the spectral form in Eq. (B1) to Eq. (B6) as follows:

$$T(\Delta, \omega; \tau_u) = \delta\Omega^8 \tilde{A}_{0_u} \tilde{A}_{0_x} \mathcal{P} \int d\Omega f_{\text{SL}}(\Omega) \quad (\text{B10})$$

where the integrand in the complex plane $f_{\text{SL}}(z)$ is defined as

$$f_{\text{SL}}(z) \equiv \frac{e^{-iz\tau_u}}{z(z-Z_+)^2(z-Z_-)^2(z-Z_+^*)^2(z-Z_-^*)^2} \quad (\text{B11})$$

$$\begin{aligned} -\frac{1}{2i\pi} T(\Delta, \omega; \tau_u) &= -\frac{1}{2i\pi} T\left(\delta\Omega s, 2\delta\Omega w; \frac{\eta}{\delta\Omega}\right) \\ &= \tilde{A}_{0_u} \tilde{A}_{0_x} \left[\theta(\tau_u) \frac{e^{-is|\eta|} e^{-|\eta|}}{64} \left\{ -\frac{ip(s, w)\Theta(w; \eta) + 2q(s, w)\Upsilon(w; \eta)}{\{1 + (s-w)^2\}\{1 + (s+w)^2\}} + Z_c(s; w) \cos(w|\eta|) + Z_s(s; w) \right. \right. \\ &\quad \left. \left. \times \frac{\sin(w|\eta|)}{w} \right\} - \theta(-\tau_u) \frac{e^{is|\eta|} e^{-|\eta|}}{64} \{ \dots \}^* \right] + \frac{1}{2} \tilde{A}_{0_u} \tilde{A}_{0_x} \{ \theta(\tau_u) - \theta(-\tau_u) \} \frac{1}{\{(s+w)^2 + 1\}^2 \{(s-w)^2 + 1\}^2}, \end{aligned} \quad (\text{B14})$$

where we define the nondimensional parameters $s \equiv \frac{\Delta}{\delta\Omega}$, $w \equiv \frac{\omega}{2\delta\Omega}$, and $\eta \equiv \delta\Omega\tau_u$. The following formulas are used in Eq. (B14):

$$p(s; w) \equiv -(s+i)(s^2+1) + (s-i)w^2, \quad (\text{B15})$$

$$q(s; w) \equiv (s+i)^2 - w^2, \quad (\text{B16})$$

$$\begin{aligned} \Theta(\eta; w) &\equiv 2 \left[(|\eta|+1) \cos(w|\eta|) + |\eta|(2|\eta|+1) \frac{\sin(w|\eta|)}{w|\eta|} + \frac{|\eta|}{w^2} \left\{ \frac{\sin(w|\eta|)}{w|\eta|} - \cos(w|\eta|) \right\} \right] \frac{1}{(1+w^2)^2} \\ &\quad + 2 \left\{ 4 \cos(w|\eta|) + 3|\eta| \frac{\sin(w|\eta|)}{w|\eta|} - w \sin(w|\eta|) \right\} \frac{1}{(1+w^2)^3}, \end{aligned} \quad (\text{B17})$$

$$\begin{aligned} \Upsilon(\eta; w) &\equiv \left[|\eta| \{ (-|\eta|+1) + (|\eta|+1)w^2 \} \frac{\sin(w|\eta|)}{w|\eta|} - (2|\eta|+1) \cos(w|\eta|) \right] \frac{1}{(1+w^2)^2} \\ &\quad - \left\{ |\eta|(1-3w^2) \frac{\sin(w|\eta|)}{w|\eta|} + (3-w^2) \cos(w|\eta|) \right\} \frac{1}{(1+w^2)^3}, \end{aligned} \quad (\text{B18})$$

and the second-order poles Z_{\pm} are given by

$$Z_{\pm} = \Delta \pm \frac{\omega}{2} + i\delta\Omega. \quad (\text{B12})$$

The integrand also contains a simple pole at $z=0$. The positions of all poles are schematically shown in Fig. 10(b). We perform the contour integral of $f_{\text{SL}}(z)$ in the complex plane by choosing a closed semicircle contour C_- to calculate $\mathcal{P} \int d\Omega f_{\text{SL}}(\Omega)$ for $\tau_u > 0$, because $|\int_{C_R^-} dz f_{\text{SL}}(z)| \rightarrow 0$ and $\int_{C_{\epsilon}^-} dz f_{\text{SL}}(z) \rightarrow \mathcal{P} \int d\Omega f_{\text{SL}}(\Omega)$ when $R \rightarrow \infty$ and $\epsilon \rightarrow 0$; thus, we evaluate $\mathcal{P} \int d\Omega f_{\text{SL}}(\Omega) = \int_{C_-} dz f_{\text{SL}}(z) - \int_{C_{\epsilon}^-} dz f_{\text{SL}}(z)$. We also evaluate $\int_{C_+} dz f_{\text{SL}}(z)$ for $\tau_u < 0$ for a similar reason. As a result, the PVI is described as the sum of the residues as

$$\begin{aligned} \mathcal{P} \int d\Omega f_{\text{SL}}(\Omega) &= -2i\pi \left[\theta(\tau_u) \left\{ \text{Res}_{z=Z_+^*} f_{\text{SL}}(z) + \text{Res}_{z=Z_-^*} f_{\text{SL}}(z) \right. \right. \\ &\quad \left. \left. + \frac{1}{2} \text{Res}_{z=0} f_{\text{SL}}(z) \right\} - \theta(-\tau_u) \{ \dots \}^* \right], \end{aligned} \quad (\text{B13})$$

where $\{ \dots \}^*$ denotes the complex conjugate of the terms in the first curly brackets. The residues other than $z=0$ always contain the damping term of $e^{-\delta\Omega|\tau_u|}$ or $|\tau_u| e^{-\delta\Omega|\tau_u|}$; thus, the right-hand side of Eq. (B13) approaches $-i\pi \{ \theta(\tau_u) - \theta(-\tau_u) \} \text{Res}_{z=0} f_{\text{SL}}(z)$ when $|\tau_u|$ is much larger than $\delta\Omega^{-1}$. The situation is similar even when Z_{\pm} are the n th poles and the residues contain the damping terms of $|\tau_u|^m e^{-\delta\Omega|\tau_u|}$, where m is an integer ranging from zero to $n-1$, as we have already explained for Eq. (32) in Sec. III B.

Substituting the calculated results of the residues into Eq. (B13) and using Eq. (B10), we can derive $-\frac{1}{2i\pi} T(\Delta, \omega; \tau_u)$ as

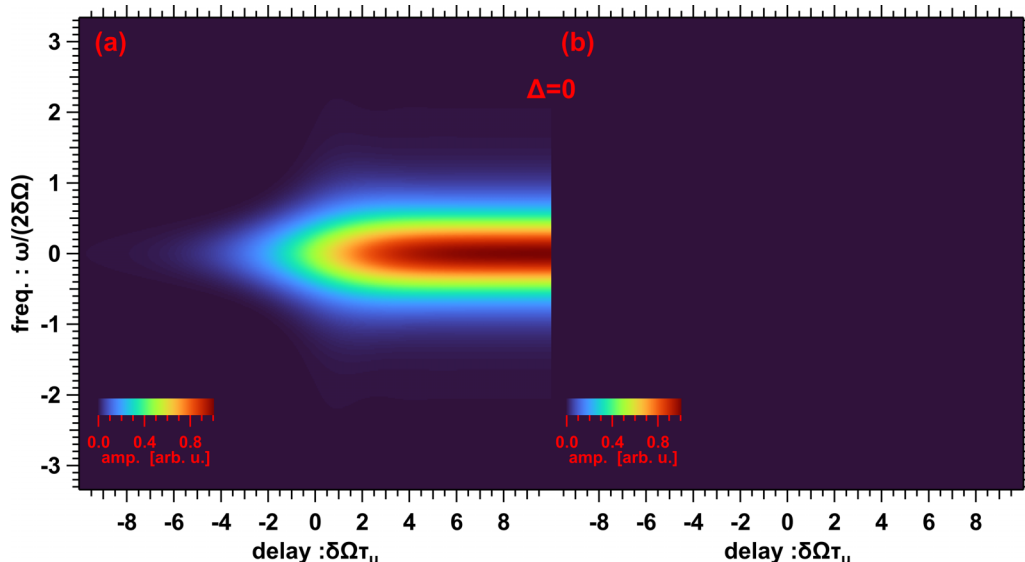


FIG. 11. Real (a) and imaginary (b) parts of the time-ordered integration amplitude $S_{ux}(\frac{\omega}{2} + \omega_u, \frac{\omega}{2} + \omega_x; \tau_u) e^{-i(\frac{\omega}{2} + \omega_u)\tau_u}$ under the resonance condition ($\Delta = s\delta\Omega = 0$). The spectral envelopes of the UV and XUV pulses are both assumed to be square Lorentz functions with the same bandwidth given by Eq. (B1).

$$Z_c(s; w) \equiv \frac{2}{(w^2 + 1)^2} \frac{w^2 + 2 + (s - 3i)^2}{(s + w - i)^2 (s - w - i)^2}, \quad (\text{B19})$$

$$Z_s(s; w) \equiv \frac{4}{(w^2 + 1)^2} \frac{\{w^2 + (s - i)^2\} + i(w^2 - 1)(s - i)}{(s + w - i)^2 (s - w - i)^2}. \quad (\text{B20})$$

The complex conjugate in the curly brackets in Eq. (B14) is denoted as $\{\dots\}^*$. The terms in the square brackets on the right-hand side of Eq. (B14) are reduced due to the exponential damping factor of $e^{-|\eta|}$ when the delay $|\eta| = \delta\Omega|\tau_u|$ is much larger than unity, and only the last term, which is equal to $\frac{1}{2}\{\theta(\tau_u) - \theta(-\tau_u)\}\tilde{A}_u(\Delta + \frac{\omega}{2})\tilde{A}_x(-\Delta + \frac{\omega}{2})$, remains. Therefore, the right-hand side of Eq. (B5) approaches $\frac{1}{2}\{1 + \theta(\tau_u) - \theta(-\tau_u)\}\tilde{A}_u(\Delta + \frac{\omega}{2})\tilde{A}_x(-\Delta + \frac{\omega}{2})$ for $\delta\Omega|\tau_u| \gg 1$, which is equivalent to Eq. (32). Substituting Eq. (B14) into Eq. (B5), we obtain the time-ordered integration amplitude.

We show the real and imaginary parts of the time-ordered integration amplitude $S_{ux}(\Delta + \frac{\omega}{2} + \omega_u, -\Delta + \frac{\omega}{2} + \omega_x; \tau_u)$, which is calculated from Eqs. (B5) and (B14) under the resonant condition of $\Delta = s\delta\Omega = 0$, in Figs. 11(a) and 11(b), respectively. We excluded the periodic phase modulation originating from $e^{-i(\frac{\omega}{2} + \omega_u)\tau_u}$ in the calculation to clearly show the alteration of the magnitude of the real part. In fact, the real part gradually emerges around $\tau_u = 0$ and retains a constant value of unity as τ_u increases within the frequency bandwidth of $\sim\delta\Omega$, whereas the imaginary part is exactly equal to zero. The real part can be regarded as a step function of τ_u with a gentle slope around $\tau_u = 0$ and expresses the sequential process caused after the irradiation of the XUV pulse.

Because the form of Eq. (B14) is general, we can also derive the asymptotic form of the time-ordered integration amplitude under the off-resonance condition, $|\Delta| \gg \delta\Omega$ ($|s| \gg 1$), by neglecting the terms involving $O(s^{-2})$ and

higher. As a result, we obtain the asymptotic form

$$-\frac{1}{2i\pi} T(\Delta, \omega; \tau_u) \simeq i\tilde{A}_{0_u}\tilde{A}_{0_x} \frac{e^{-is\eta} e^{-|\eta|}}{64} \frac{\Theta(w; \eta)}{s} = -\frac{1}{2i\pi} \frac{T_{\text{FROG}_{ux}}(\omega; \tau_u)}{\Delta}, \quad (\text{B21})$$

where $T_{\text{FROG}_{ux}}(\omega; \tau_u)$ is obtained by substituting Eq. (B1) into Eq. (B9):

$$T_{\text{FROG}_{ux}}(\omega; \tau_u) = T_{\text{FROG}_{ux}}\left(\delta\Omega w; \frac{\eta}{\delta\Omega}\right) = 2\pi\delta\Omega\tilde{A}_{0_u}\tilde{A}_{0_x} \frac{e^{-is\eta} e^{-|\eta|}}{64} \Theta(w; \eta), \quad (\text{B22})$$

The asymptotic form of Eq. (B21) is consistent with Eq. (B8) derived without determining the specific forms of $\tilde{A}_u(\Omega)$ and $\tilde{A}_x(\Omega)$. We calculate $S_{ux}(\Delta + \frac{\omega}{2} + \omega_u, -\Delta + \frac{\omega}{2} + \omega_x; \tau_u) e^{-i(\Delta + \frac{\omega}{2} + \omega_u)\tau_u}$ in Eq. (B5) using Eq. (B14) by setting $\Delta = 2.5\delta\Omega$ to simulate the off-resonance condition, as shown in Figs. 12(a) and 12(b). The structures of the images in these figures are entirely different from those in Figs. 11(a) and 11(b). Different from the resonant condition, the amplitude of the imaginary part is much larger than that of the real part and they are both restricted only in the delay range at around zero. The peak amplitude of the imaginary part is less than 10% of that of the real part under the resonant condition. The amplitude emerges only when the XUV and UV pulses temporally overlap, and thus this result expresses a nonsequential two-photon process independent of the molecular effect originating from the time order of the two optical pulses. In fact, the magnitude square of the amplitude shown in Fig. 12(c), which is calculated from the real and imaginary parts in Figs. 12(a) and 12(b), is very similar to the FROG image calculated from $|T_{\text{FROG}_{ux}}(\omega; \tau_u)|^2$ in Eq. (B22), as shown in Fig. 12(d), and thus the spectral alteration of the continuum electron upon a scanning delay τ_u mainly reveals

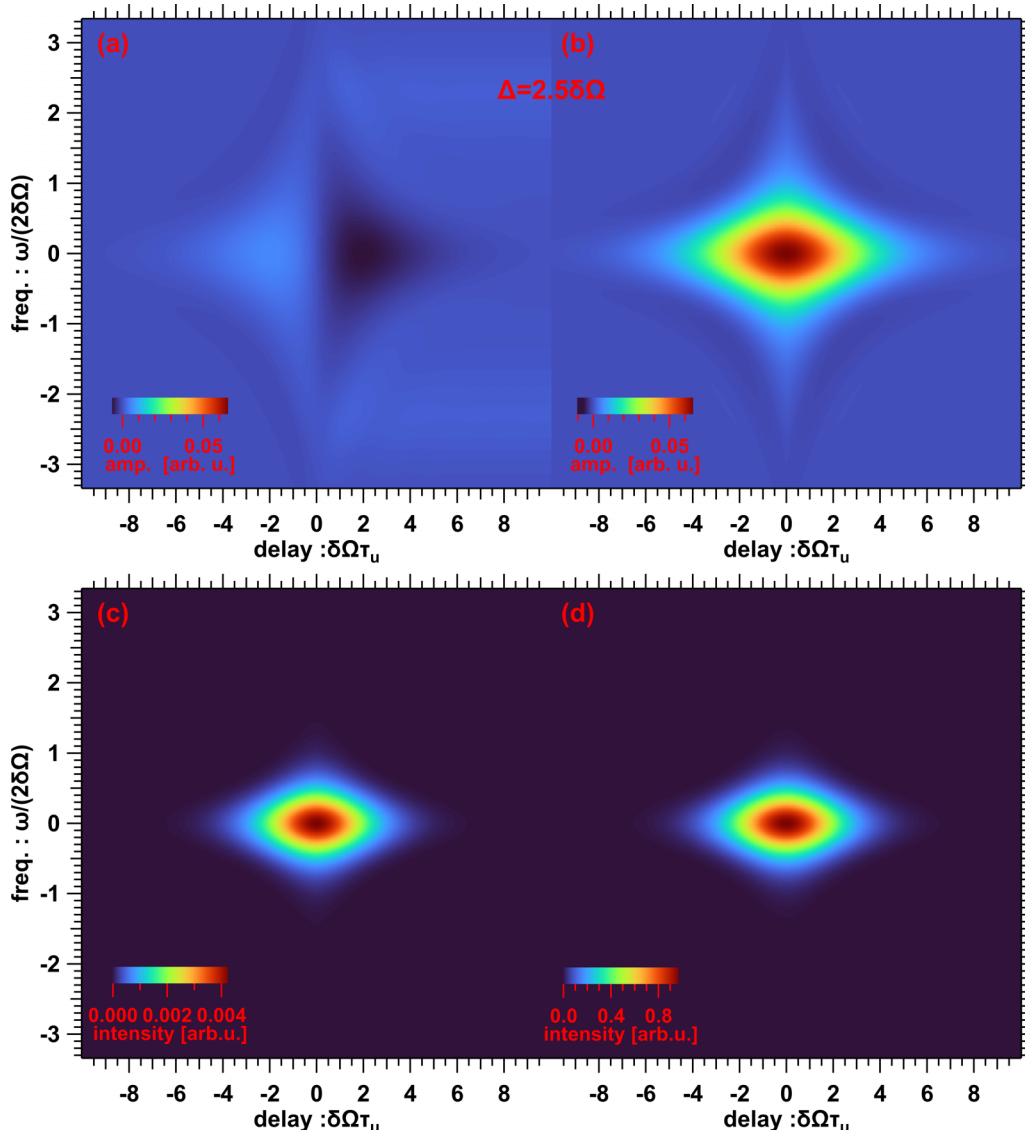


FIG. 12. Real (a) and imaginary (b) parts of the time-ordered integration amplitude $S_{ux}(\Delta + \frac{\omega}{2} + \omega_u, -\Delta + \frac{\omega}{2} + \omega_x; \tau_u) e^{-i(\Delta + \frac{\omega}{2} + \omega_u)\tau_u}$ under the off-resonance condition ($\Delta = 2.5\delta\Omega$). (c) Magnitude square of the time-ordered integration amplitude calculated from the amplitude shown in (a) and (b). (d) FROG image calculated from $|T_{\text{FROG}_{ux}}(\omega; \tau_u)|^2$ in Eq. (B22). The spectral envelopes of the UV and XUV pulses are both assumed to be square Lorentz functions with the same bandwidth given by Eq. (B1).

the characteristics of the optical pulses rather than those of the dynamical evolution of a target molecule.

We suppose at present that the successful observation of the autocorrelation signals of APTs on the ion fragments yielded from nitrogen molecules [32] and acetylene molecules [19] in past experiments was owing to the off-resonance condition resulting in nonsequential processes, and we attribute the appearance of the vibration-motional signals of hydrogen molecular ions on H^+ yielded from hydrogen molecules [20–22] to the resonance in the excitation from the $1s\sigma_g$ state to the $2p\sigma_u$ state in H_2^+ , which was regarded as a sequential process after photoionization, even though we utilized the same light source to deliver a pair of APTs for the experiments targeting these three kinds of molecule.

2. Gaussian function

When we assume the spectral envelopes of $\tilde{A}_u(\Omega)$ and $\tilde{A}_x(\Omega)$ to be Gaussian functions such as

$$\tilde{A}_{u,x}(\Omega) = \tilde{A}_{0u,x} e^{-\frac{\Omega^2}{\delta\Omega_{u,x}^2}}, \quad (\text{B23})$$

the temporal profiles of the envelope functions are also the following Gaussian function of time t :

$$A_{u,x}(t) = \frac{\delta\Omega_{u,x}\tilde{A}_{0u,x}}{2\sqrt{\pi}} e^{-\frac{\delta\Omega_{u,x}^2}{4}t^2}, \quad (\text{B24})$$

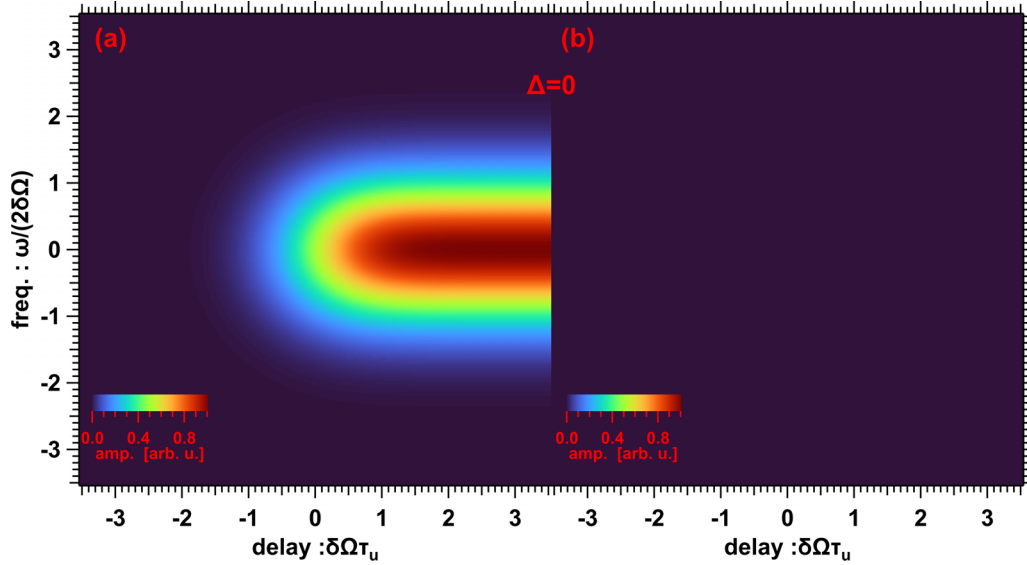


FIG. 13. Real (a) and imaginary (b) parts of the time-ordered integration amplitude $S_{ux}(\frac{\omega}{2} + \omega_u, \frac{\omega}{2} + \omega_x; \tau_u) e^{-i(\frac{\omega}{2} + \omega_u)\tau_u}$ under the resonance condition ($\Delta = s\delta\Omega = 0$). The spectral envelopes of the UV and XUV pulses are both assumed to be Gaussian functions with the same bandwidth given by Eq. (B23).

where we define the bandwidths of the UV and XUV pulses as $\delta\Omega_u$ and $\delta\Omega_x$, respectively. We introduce the following spectral peak difference ω and detuning Δ in a similar manner to Eqs. (B3) and (B4):

$$\begin{aligned} \omega &\equiv \Omega_1 + \Omega_2 - \omega_u - \omega_x \\ &= \omega'_e - \left\{ \omega_u + \omega_x - (\kappa' + \kappa_0 - \omega_g^0) \right\}, \end{aligned} \quad (\text{B25})$$

$$\begin{aligned} \Delta &\equiv \alpha_u(\Omega_1 - \omega_u) - \alpha_x(\Omega_2 - \omega_x) \\ &= \alpha_u(\kappa' + \kappa_0 - \omega^{+v'} - \omega_u) \\ &\quad - \alpha_x(\omega'_e + \omega^{+v'} - \omega_g^0 - \omega_x), \end{aligned} \quad (\text{B26})$$

where we define the coefficients $\alpha_u \equiv \delta\Omega_u^{-2}/(\delta\Omega_u^{-2} + \delta\Omega_x^{-2})$ and $\alpha_x \equiv \delta\Omega_x^{-2}/(\delta\Omega_u^{-2} + \delta\Omega_x^{-2})$ and the following bandwidth of the envelope product $\delta\Omega_{ux}$:

$$\delta\Omega_{ux} \equiv \left(\frac{1}{\delta\Omega_u^2} + \frac{1}{\delta\Omega_x^2} \right)^{-\frac{1}{2}}. \quad (\text{B27})$$

Then, we find that the product of the two spectral amplitudes can be rewritten in the form of $\tilde{A}_u(\Omega_1 - \omega_u - \Omega)\tilde{A}_x(\Omega_2 - \omega_x + \Omega) = \tilde{A}_u\tilde{A}_x e^{-\frac{\omega^2}{\delta\Omega_u^2 + \delta\Omega_x^2}} e^{-\frac{(\Omega - \Delta)^2}{\delta\Omega_{ux}^2}}$, and the time-ordered integration amplitude is expressed in terms of Δ and ω as

$$\begin{aligned} S_{ux}(\Omega_1, \Omega_2; \tau_u) e^{-i\Omega_1\tau_u} \\ = -\frac{1}{2i\pi} T(\Delta, \omega; \tau_u) + \frac{1}{2} \tilde{A}_u\tilde{A}_x e^{-\frac{\omega^2}{\delta\Omega_u^2 + \delta\Omega_x^2}} e^{-\frac{\Delta^2}{\delta\Omega_{ux}^2}}. \end{aligned} \quad (\text{B28})$$

We use the relations $\Omega_1 = \frac{\alpha_x\omega}{\alpha_u + \alpha_x} + \frac{\Delta}{\alpha_u + \alpha_x} + \omega_u$ and $\Omega_2 = \frac{\alpha_u\omega}{\alpha_u + \alpha_x} - \frac{\Delta}{\alpha_u + \alpha_x} + \omega_x$ to find Eq. (B28). The amplitude $T(\Delta, \omega; \tau_u)$ is given by

$$T(\Delta, \omega; \tau_u) = \tilde{A}_u\tilde{A}_x e^{-\frac{\omega^2}{\delta\Omega_u^2 + \delta\Omega_x^2}} \mathcal{P} \int d\Omega \frac{e^{-\frac{(\Omega - \Delta)^2}{\delta\Omega_{ux}^2}} e^{-i\Omega\tau_u}}{\Omega}$$

$$\begin{aligned} &= 2\sqrt{\pi}\tilde{A}_u\tilde{A}_x e^{-\frac{\omega^2}{\delta\Omega_u^2 + \delta\Omega_x^2}} e^{-\frac{\delta\Omega_{ux}^2}{4}\tau_u^2} e^{-i\Delta\tau_u} \\ &\quad \times D_+ \left(\frac{\Delta}{\delta\Omega_{ux}} - i\frac{\delta\Omega_{ux}}{2}\tau_u \right), \end{aligned} \quad (\text{B29})$$

where we have introduced the Dawson function $D_+(x) = e^{-x^2} \int_0^x dx' e^{x'^2}$. Note that the Ω integral in Eq. (B29) can be implemented after differentiating the integrand with respect to τ_u to remove the pole at $\Omega = 0$, and then we obtain a Gaussian function of τ_u . The resultant Gaussian function of τ_u is integrated again with the initial condition at $\tau_u = 0$, which is calculated by the Hilbert transform of the Gaussian function of Δ . Accordingly, we obtain the equation on the right-hand side of the last line in Eq. (B29).

To simulate the resonance condition, the amplitude $T(\Delta, \omega; \tau_u)$ in Eq. (B29) is transformed to

$$\begin{aligned} T(\Delta = 0, \omega; \tau_u) \\ = -i\pi\tilde{A}_u\tilde{A}_x e^{-\frac{\omega^2}{\delta\Omega_u^2 + \delta\Omega_x^2}} \operatorname{erf} \left(\frac{\delta\Omega_{ux}}{2}\tau_u \right), \end{aligned} \quad (\text{B30})$$

where we have used the relation $e^{-s^2} D_+(-is) = -i\frac{\sqrt{\pi}}{2} \operatorname{erf}(s)$. Substituting Eq. (B30) into Eq. (B28), the time-ordered integration amplitude becomes

$$\begin{aligned} S_{ux} \left(\frac{\alpha_x\omega}{\alpha_u + \alpha_x} + \omega_u, \frac{\alpha_u\omega}{\alpha_u + \alpha_x} + \omega_x; \tau_u \right) e^{-i(\frac{\alpha_x\omega}{\alpha_u + \alpha_x} + \omega_u)\tau_u} \\ = \frac{1}{2} \left\{ \operatorname{erf} \left(\frac{\delta\Omega_{ux}}{2}\tau_u \right) + 1 \right\} \tilde{A}_u\tilde{A}_x e^{-\frac{\omega^2}{\delta\Omega_u^2 + \delta\Omega_x^2}}. \end{aligned} \quad (\text{B31})$$

The time-ordered integration amplitude in Eq. (B31) is a step function of τ_u with a gentle slope around $\tau_u = 0$ and exhibits the Gaussian distribution with respect to the peak difference ω . These characteristics are consistent with the general asymptotic formula in Eq. (32).

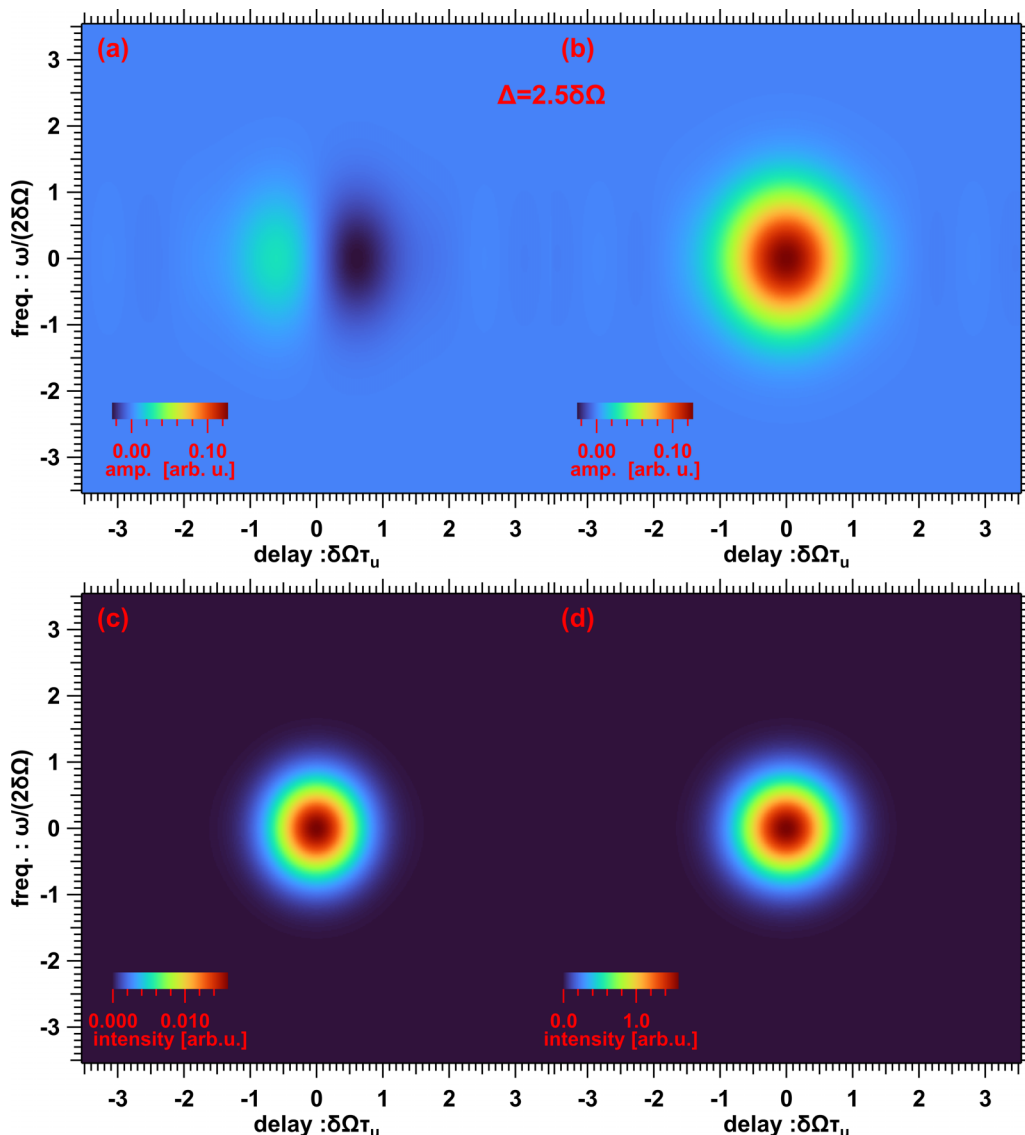


FIG. 14. Real (a) and imaginary (b) parts of the time-ordered integration amplitude $S_{ux}(\Delta + \frac{\omega}{2} + \omega_u, -\Delta + \frac{\omega}{2} + \omega_x; \tau_u) e^{-i(\Delta + \frac{\omega}{2} + \omega_u)\tau_u}$ under the off-resonance condition ($\Delta = 2.5\delta\Omega$). (c) Magnitude square of the time-ordered integration amplitude calculated from the amplitude shown in (a) and (b). (d) FROG image calculated from $|T_{\text{FROG}_{ux}}(\omega; \tau_u)|^2$ in Eq. (B33). The spectral envelopes of the UV and XUV pulses are both assumed to be Gaussian functions with the same bandwidth given by Eq. (B23).

When we consider the off-resonance condition that the detuning $|\Delta|$ is much larger than $\delta\Omega_{ux}$ ($|\Delta| \gg \delta\Omega_{ux}$), we have to classify the region of τ_u into two. In the region $\delta\Omega_{ux}|\tau_u| \lesssim 1$, the inequalities $\delta\Omega_{ux}^2|\tau_u| \lesssim \delta\Omega_{ux} \ll |\Delta|$ are satisfied, ensuring that the conditions $\frac{|\Delta|}{\delta\Omega_{ux}} \gg 1$ and $\frac{|\Delta|}{\delta\Omega_{ux}} \gg \frac{\delta\Omega_{ux}}{2}|\tau_u|$ are both satisfied. Thus, we neglect the imaginary part of the argument in the Dawson function in Eq. (B29) and adopt the asymptotic form $D_+(x) \simeq \frac{1}{2x}$ for a real variable of x with a large magnitude [34]. We express the resultant asymptotic form of the amplitude $T(\Delta, \omega; \tau_u)$ as follows:

$$\begin{aligned}
 T(\Delta, \omega; \tau_u) & \\
 & \simeq \frac{1}{\Delta} \sqrt{\pi} \delta\Omega_{ux} \tilde{A}_{0_u} \tilde{A}_{0_x} e^{-\frac{\omega^2}{\delta\Omega_u^2 + \delta\Omega_x^2}} e^{-\frac{\delta\Omega_{ux}^2}{4} \tau_u^2} e^{-i\Delta\tau_u} \\
 & = \frac{1}{\Delta} T_{\text{FROG}_{ux}}(\omega; \tau_u) e^{i(\frac{\alpha_u\omega}{\alpha_u + \alpha_x} - \frac{\Delta}{\alpha_u + \alpha_x})\tau_u}, \quad (\text{B32})
 \end{aligned}$$

where the FROG amplitude $T_{\text{FROG}_{ux}}(\omega; \tau_u)$ is derived by substituting Eq. (B23) into Eq. (B9):

$$\begin{aligned}
 T_{\text{FROG}_{ux}}(\omega; \tau_u) & \\
 & = \sqrt{\pi} \delta\Omega_{ux} \tilde{A}_{0_u} \tilde{A}_{0_x} e^{-\frac{\omega^2}{\delta\Omega_u^2 + \delta\Omega_x^2}} e^{-\frac{\delta\Omega_{ux}^2}{4} \tau_u^2} e^{-i(\frac{\alpha_u\omega}{\alpha_u + \alpha_x} - \frac{\Delta}{\alpha_u + \alpha_x} + \Delta)\tau_u}. \quad (\text{B33})
 \end{aligned}$$

In the region $\delta\Omega_{ux}|\tau_u| \gtrsim 1$, the Dawson function diverges with increasing $|\tau_u|$. Nevertheless, the decrease in the magnitude by multiplying the Gaussian function $e^{-\frac{\delta\Omega_{ux}^2}{4} \tau_u^2}$ is more pronounced than the divergence of the Dawson function. Thus, we conclude that $T(\Delta, \omega; \tau_u) \approx 0$ for $\delta\Omega_{ux}|\tau_u| \gg 1$ and that the asymptotic form in Eq. (B32) is still applicable. Substituting Eq. (B32) into Eq. (B28), we confirm that the resultant S_{ux} is consistent with the general asymptotic form in Eq. (B8).

We show the real and imaginary parts of the time-ordered integration amplitude, which is calculated from Eqs. (B28) and (B29) under the resonance condition of $\Delta = 0$, in Figs. 13(a) and 13(b), respectively. We assume the bandwidths of the UV and XUV pulses to be the same ($\delta\Omega_u = \delta\Omega_x = \delta\Omega$) in this calculation for simplicity. The principal characteristics of the images in these figures are the same as those of the images in Figs. 11(a) and 11(b), namely, the steplike evolution regarding the delay τ_u with a gentle slope around $\tau_u = 0$ and the localization within the frequency bandwidth in the real part, with no contribution from the imaginary part.

The similarity of the images calculated from the Gaussian spectral envelope functions to those calculated from the square Lorentz spectral envelope functions is retained even when the off-resonance condition is applied to Eq. (B29). The real part of the time-ordered integration amplitude with $\Delta = 2.5\delta\Omega$ shown in Fig. 14(a) exhibits significantly small

positive and negative peak magnitudes compared with the peak magnitude of the imaginary part shown in Fig. 14(b), although the peak magnitude is only $\approx 12.5\%$ of the maximum magnitude of the real part under the resonance condition. The imaginary part is confined around the origin for both the delay and frequency directions, in contrast to the constant magnitude of the real part demonstrated in the large positive delay range under the resonance condition. In addition, we confirm that the approximated formula of Eq. (B32) is reasonable by comparing the magnitude square of the time-ordered integration amplitude and the magnitude square of the FROG amplitude $|T_{\text{FROG}_{\text{ux}}}(\omega; \tau_u)|^2$, as shown in Figs. 14(c) and 14(d), respectively.

Even though we do not present a general proof of the approximated formula of Eq. (32), we show that this formula is applicable for feasible analytical functions adopted as a model of the spectral envelope of an optical pulse.

-
- [1] D. W. Turner and D. P. May, Franck-Condon factors in ionization: Experimental measurement using molecular photoelectron spectroscopy, *J. Chem. Phys.* **45**, 471 (1966).
- [2] M. A. Nielsen and I. L. Chuang, *Quantum Computation and Quantum Information*, 10th ed. (Cambridge University, New York, 2016).
- [3] D. W. Turner, C. Baker, A. D. Baker, and C. R. Brundle, *Molecular Photoelectron Spectroscopy* (Wiley, New York, 1970).
- [4] M. J. J. Vrakking, Control of Attosecond Entanglement and Coherence, *Phys. Rev. Lett.* **126**, 113203 (2021).
- [5] E. Goulielmakis, Z.-H. Loh, A. Wirth, R. Santra, N. Rohringer, V. S. Yakovlev, S. Zherebtsov, T. Pfeifer, A. M. Azzeer, M. F. Kling, S. R. Leone, and F. Krausz, Real-time observation of valence electron motion, *Nature (London)* **466**, 739 (2010).
- [6] S. Pabst, M. Lein, and H. J. Wörner, Preparing attosecond coherences by strong-field ionization, *Phys. Rev. A* **93**, 023412 (2016).
- [7] S. Carlström, J. Mauritsson, K. J. Schafer, A. L'Huillier, and M. Gisselbrecht, Quantum coherence in photo-ionisation with tailored XUV pulses, *J. Phys. B* **51**, 015201 (2018).
- [8] M. Ruberti, Onset of ionic coherence and ultrafast charge dynamics in attosecond molecular ionisation, *Phys. Chem. Chem. Phys.* **21**, 17584 (2019).
- [9] S. Pabst, L. Greenman, P. J. Ho, D. A. Mazziotti, and R. Santra, Decoherence in Attosecond Photoionization, *Phys. Rev. Lett.* **106**, 053003 (2011).
- [10] C. Arnold, O. Vendrell, and R. Santra, Electronic decoherence following photoionization: Full quantum-dynamical treatment of the influence of nuclear motion, *Phys. Rev. A* **95**, 033425 (2017).
- [11] M. Vacher, M. J. Bearpark, M. A. Robb, and J. P. Malhado, Electron Dynamics upon Ionization of Polyatomic Molecules: Coupling to Quantum Nuclear Motion and Decoherence, *Phys. Rev. Lett.* **118**, 083001 (2017).
- [12] D. Schwickert, M. Ruberti, P. Kolorenč, S. Usenko, A. Przystawik, K. Baev, I. Baev, M. Braune, L. Bocklage, M. K. Czwalińska, S. Deinert, S. Düsterer, A. Hans, G. Hartmann, C. Haunhorst, M. Kuhlmann, S. Palutke, R. Röhlberger, J. Rönsch-Schulenburg, P. Schmidt *et al.*, Electronic quantum coherence in glycine molecules probed with ultrashort x-ray pulses in real time, *Sci. Adv.* **8**, eabn6848 (2022).
- [13] E. J. Heller, The semiclassical way to molecular spectroscopy, *Acc. Chem. Res.* **14**, 368 (1981).
- [14] G. A. Fiete and E. J. Heller, Semiclassical theory of coherence and decoherence, *Phys. Rev. A* **68**, 022112 (2003).
- [15] T. Nishi, E. Lötstedt, and K. Yamanouchi, Entanglement and coherence in photoionization of H₂ by an ultrashort XUV laser pulse, *Phys. Rev. A* **100**, 013421 (2019).
- [16] M. Ruberti, Quantum electronic coherences by attosecond transient absorption spectroscopy: *Ab initio* b-spline RCS-ADC study, *Faraday Discuss.* **228**, 286 (2021).
- [17] M. Ruberti, S. Patchkovskii, and V. Averbukh, Quantum coherence in molecular photoionization, *Phys. Chem. Chem. Phys.* **24**, 19673 (2022).
- [18] M. J. J. Vrakking, Ion-photoelectron entanglement in photoionization with chirped laser pulses, *J. Phys. B* **55**, 134001 (2022).
- [19] T. Matsubara, S. Fukahori, E. Lötstedt, Y. Nabekawa, K. Yamanouchi, and K. Midorikawa, 300attosecond response of acetylene in two-photon ionization/dissociation processes, *Optica* **8**, 1075 (2021).
- [20] Y. Furukawa, Y. Nabekawa, T. Okino, A. A. Eilanlou, E. J. Takahashi, P. Lan, K. L. Ishikawa, T. Sato, K. Yamanouchi, and K. Midorikawa, Resolving vibrational wave-packet dynamics of D₂ using multicolor probe pulses, *Opt. Lett.* **37**, 2922 (2012).
- [21] Y. Nabekawa, Y. Furukawa, T. Okino, A. A. Eilanlou, E. J. Takahashi, K. Yamanouchi, and K. Midorikawa, Settling time of a vibrational wavepacket in ionization, *Nat. Commun.* **6**, 8197 (2015).
- [22] Y. Nabekawa, Y. Furukawa, T. Okino, A. A. Eilanlou, E. J. Takahashi, K. Yamanouchi, and K. Midorikawa, Sub-10-fs control of dissociation pathways in the hydrogen molecular ion with a few-pulse attosecond pulse train, *Nat. Commun.* **7**, 12835 (2016).
- [23] T. Okino, Y. Furukawa, Y. Nabekawa, and K. Midorikawa, Multi-photon dissociative ionization of D₂ probed by a few-pulse attosecond pulse train, in *2017 European Conference on Lasers and Electro-Optics and European Quantum Electronics Conference* (Optica Publishing Group, 2017), p. CG_7_5.

- [24] Y. Nabekawa, A. Amani Eilanlou, Y. Furukawa, K. L. Ishikawa, H. Takahashi, and K. Midorikawa, Multi-terawatt laser system generating 12-fs pulses at 100 Hz repetition rate, *Appl. Phys. B* **101**, 523 (2010).
- [25] T. Matsubara, Y. Nabekawa, K. L. Ishikawa, K. Yamanouchi, and K. Midorikawa, Attosecond optical and Ramsey-type interferometry by postgeneration splitting of harmonic pulse, *Ultrafast Sci.* **2022**, 9858739 (2022).
- [26] A. Matsuda, M. Fushitani, C.-M. Tseng, Y. Hikosaka, J. H. D. Eland, and A. Hishikawa, A magnetic-bottle multi-electron ion coincidence spectrometer, *Rev. Sci. Instrum.* **82**, 103105 (2011).
- [27] M. Fushitani, Y. Sasaki, A. Matsuda, H. Fujise, Y. Kawabe, K. Hashigaya, S. Owada, T. Togashi, K. Nakajima, M. Yabashi, Y. Hikosaka, and A. Hishikawa, Multielectron-Ion Coincidence Spectroscopy of Xe in Extreme Ultraviolet Laser Fields: Non-linear Multiple Ionization via Double Core-Hole States, *Phys. Rev. Lett.* **124**, 193201 (2020).
- [28] M. Fushitani, M. Yamada, H. Fujise, S. Owada, T. Togashi, K. Nakajima, M. Yabashi, A. Matsuda, Y. Hikosaka, and A. Hishikawa, Capturing transient core-to-core resonances in Kr in intense extreme-ultraviolet laser fields by electron-ion coincidence spectroscopy, *Phys. Rev. A* **107**, L021101 (2023).
- [29] T. Nakajima and Y. Fujimura, *Basics of Modern Quantum Chemistry* (Kyoritsu, Tokyo, 1999).
- [30] D. J. Kane, G. Rodriguez, A. J. Taylor, and T. S. Clement, Simultaneous measurement of two ultrashort laser pulses from a single spectrogram in a single shot, *J. Opt. Soc. Am. B* **14**, 935 (1997).
- [31] R. Trebino, K. W. DeLong, D. N. Fittinghoff, J. N. Sweetser, M. A. Krumbügel, B. A. Richman, and D. J. Kane, Measuring ultrashort laser pulses in the time-frequency domain using frequency-resolved optical gating, *Rev. Sci. Instrum.* **68**, 3277 (1997).
- [32] T. Okino, Y. Furukawa, Y. Nabekawa, S. Miyabe, A. Amani Eilanlou, E. J. Takahashi, K. Yamanouchi, and K. Midorikawa, Direct observation of an attosecond electron wave packet in a nitrogen molecule, *Sci. Adv.* **1**, e1500356 (2015).
- [33] Y. Nabekawa and K. Midorikawa, Interferometric autocorrelation of an attosecond pulse train calculated using feasible formulae, *New J. Phys.* **10**, 025034 (2008).
- [34] W. J. Cody, K. A. Paciorek, and H. C. Thacher, Chebyshev approximations for Dawson's integral, *Math. Comput.* **24**, 171 (1970).